

---

# REVISITING THE PREDICTABILITY OF DYNAMICAL SYSTEMS: A NEW LOCAL DATA-DRIVEN APPROACH

---

**Chenyu Dong**

College of Design and Engineering  
National University of Singapore  
chenyu.dong@u.nus.edu

**Davide Faranda**

LSCE, Université Paris-Saclay, France  
London Mathematical Laboratory, UK  
IPSL, École Normale Supérieure, France  
davide.faranda@lsce.ipsl.fr

**Adriano Gualandi**

Department of Earth Sciences  
University of Cambridge  
Istituto Nazionale di Geofisica e Vulcanologia  
ag2347@cam.ac.uk

**Valerio Lucarini**

School of Computing and Mathematical Sciences  
University of Leicester, UK  
v.lucarini@leicester.ac.uk

**Gianmarco Mengaldo\***

College of Design and Engineering  
National University of Singapore  
mpegim@nus.edu.sg

## ABSTRACT

Nonlinear dynamical systems are ubiquitous in nature and they are hard to forecast. Not only they may be sensitive to small perturbations in their initial conditions, but they are often composed of processes acting at multiple scales. Classical approaches based on the Lyapunov spectrum rely on the knowledge of the dynamic forward operator, or of a data-derived approximation of it. This operator is typically unknown, or the data are too noisy to derive a faithful representation. Here, we propose a new data-driven approach to analyze the local predictability of dynamical systems. This method, based on the concept of recurrence, is closely linked to the well-established framework of local dynamical indices. Applied to both idealized systems and real-world datasets, this new index shows results consistent with existing knowledge, proving its effectiveness in estimating local predictability. Additionally, we discuss its relationship with local dynamical indices, illustrating how it complements the previous framework as a more direct measure of predictability. Furthermore, we explore its reflection of the scale-dependent nature of predictability, its extension that includes a weighting strategy, and its real-time application. We believe these aspects collectively demonstrate its potential as a powerful diagnostic tool for complex systems.

**Keywords** Predictability · Dynamical Systems · Data-driven Methods · Local Dynamical Indices

## 1 Introduction

Systems that evolve in time according to specific rules are known as *dynamical systems*, and the associated field of study is called *dynamical system theory*. There is a rich history on this topic, starting from the 1600s, when Newton developed calculus and classical mechanics [1], to the 1800s, when Poincaré developed geometrical approaches to the study of dynamical systems [2]. In the 1900s, the field flourished, with the pioneering contributions of Birkhoff, Kolmogorov, Moser, Arnold, Lorenz, Ruelle, Takens, May, and Feigenbaum, among others, who laid the foundations of modern dynamical system theory, including works on oscillators, chaos and fractals, well summarized by Strogatz [3].

Many real-world systems are made of multiple interacting parts, giving rise to complex dynamical systems. A paradigm for describing such systems relies on considering high-dimensional deterministic models, which are often characterised by chaotic behaviour and multiscale dynamics [4, 5]. A separate paradigm relies on considering stochastic dynamics, where randomness is explicitly introduced in the system [6, 7]. When constructing reduced order models of high dimensional systems, stochastic dynamics is an emergent property. This is at the core of the Hasselmann’s program for climate science [8, 9] and can be rigorously justified thanks to the Mori-Zwanzig theory [10, 11]. The latter also lays the foundation for the use of data-driven methods aimed at estimating the role of the unresolved scales of motion on the resolved ones [12]. And, indeed, low-dimensional stochastic models have proved very valuable tools for understanding the statistical and dynamical properties of complex systems, e.g. in the area of Earth system science [13, 14, 15, 16, 17, 18].

Either way, a well-known fact is that we currently observe a finite predictability horizon for systems of interest like, for example, the atmosphere [19, 20]. This means that, when forecasting the future behaviour of a dynamical system, the error that we make tends to increase the longer into the future we want to forecast [21].

To understand predictability and the methods commonly used to assess it, we look at the evolution of the system in the so-called phase space, that is the space of all the variables used to describe it. In the phase space, usually we can identify a subset, namely a finite-size manifold of trajectories followed by the dynamical system over time and denoted by  $\mathbf{x}(t)$ , where  $\mathbf{x}$  is the vector of observables that depends on time  $t$ . This finite-size manifold is also known as attractor (random attractor in the case of stochastic dynamical systems [22]).

The origin of this practical unpredictability may stem either from an intrinsic stochastic nature of the system or from the ignorance of the current state of the system and/or of the dynamic rule controlling its evolution [23] or from a combination of both. Furthermore, it is well-known that even low-dimensional nonlinear systems may be difficult to forecast if they exhibit an exponential divergence of close-by states [19]. In such cases the unpredictability comes from our lack of precise knowledge of the current state of the system: if we knew exactly the initial conditions we would always get the same future evolution. A common quantity used to characterize the predictability of a system is the maximum Lyapunov exponent  $\lambda_{\max}$ . If we look at the evolution of two trajectories starting from two points close to each other, namely  $\mathbf{x}(t_0)$  and  $\mathbf{x}(t_0) + \delta\mathbf{x}$ , these will diverge exponentially fast as time progresses, until their distance will plateau around a value bounded by the diameter of the attractor [24]. Even more instructive is to look at the evolution of a ball around the state  $\mathbf{x}(t)$ . From this, one can define a full Lyapunov spectrum, made of Lyapunov exponents equal in number to the number of variables used to describe the phase space. The Lyapunov exponents are mean logarithmic growth rates of the lengths of the principal axes of this ball evolving under the action of the dynamic rule [25, 4, 24, 5]. The existence of at least one positive Lyapunov exponent is the hallmark of chaotic dynamical systems. Therefore, measuring predictability in dynamical systems can be re-framed as computing the divergence of a system’s trajectories over time.

It is important to highlight that the Lyapunov exponents are averaged quantities and the average is typically performed over a long trajectory. As a consequence, they serve as key indicators of the system’s global predictability [25, 4], where the term *global* refers to average properties of the system, hence to the average predictability of the system. While the average predictability of the system can be useful, theoretical curiosity as well as operational requirements and priorities indicate the need to investigate a local notion of predictability. Indeed, the stability properties of a dynamical system can be dramatically state-dependent [26]. We then wish to understand the system’s predictability in a specific region of the phase space (we will refer to these local characteristics also as *instantaneous*, since they refer to a specific time) [27, 28]. This notion has extreme relevance in the context of weather prediction [29] and key implications for devising efficient and accurate data assimilation methods [30].

To this end, local (or finite-time) Lyapunov exponents [31, 32, 28, 33] are useful quantities. However, their reliance on linearized dynamics prevents the characterization of the system outside the linear regime of perturbations. Acknowledging this limitation, finite-size Lyapunov exponents [34, 35] and nonlinear local Lyapunov exponents [36, 37] were subsequently proposed to quantify local predictability in the nonlinear regime, as they consider finite perturbations. Nonetheless, it is noteworthy that they both assume an exponential law for error growth. Although this is consistent with classic Lyapunov exponents within the linear regime, this assumption often does not hold in the nonlinear regime (i.e., for finite errors). These local indices have been applied successfully to various dynamical systems of varied complexity to gain insights into their predictability [36, 38, 34, 32], despite the aforementioned limitations.

Besides Lyapunov exponents and their variants, information theory also offers methods to quantify predictability [39, 23]. Within this framework, various entropy-based indicators are usually employed as predictability measures for model-based prediction, with varying degree of success [40, 41, 42, 43]. However, because these methods are model-based, they are unsuitable for observational datasets. Other indices from nonlinear time series analysis also use predictability measures such as sample entropy, permutation entropy, and others [44, 45, 46]; nevertheless, they are only effective

with time series or systems with relatively low dimensionality. To the best of the authors' knowledge, no information theory method can infer local predictability information from high-dimensional observational data.

From the brief review of relevant literature just outlined, the above mentioned indices have several drawbacks. More specifically, Lyapunov exponents and their variants may not work well for nonlinear regimes, while information-theory-based methods may not be applicable to high-dimensional dynamical systems. In the next section, we leverage a recent framework proposed by Lucarini et al., [47], that blends extreme value theory [47] and the Poincaré recurrence theorem [2] to build a new local predictability approach.

## A local data-driven approach

Lucarini et al., [47] introduced a novel framework to measure the local properties of dynamical systems. In particular, they combine extreme value theory [48] and the Poincaré recurrence theorem [2] to construct purely data-driven local dynamical indices, that can measure the local dimension of dynamical systems and their persistence at any point in time. Under the ergodic assumption, the Poincaré recurrence theorem guarantees that the system will visit an arbitrarily small neighborhood of any state again and again as time passes. In this methodology, for one given state of interest  $\zeta = \mathbf{x}(t = t_\zeta)$  in the phase space, its neighboring states, also known as *recurrences*, are used to characterize its local dynamical properties. To achieve this, we first define negative logarithmic returns as:

$$g(\zeta, \mathbf{x}(t)) = -\log[\text{dist}(\mathbf{x}(t), \zeta)], \quad (1)$$

where the dist function can be any distance metric. We note that requiring a trajectory falls within a neighborhood of  $\zeta$  (intended as a ball) is a synonym of having the time series  $g[\zeta, \mathbf{x}(t)]$  above one threshold  $s(q, \zeta)$ , where  $s(q, \zeta)$  is a high threshold associated to a quantile  $q$  of the series  $X \equiv g(x(t))$ .

Then, we define a quantity called *exceedance* for the neighboring states (i.e., recurrences) of  $\zeta$  as follows:

$$\mathbf{u}(\zeta) = g(\zeta, \mathbf{x}(t)) - s(q, \zeta), \quad \forall g(\zeta, \mathbf{x}(t)) > s(q, \zeta) \quad (2)$$

According to extreme value theory [49, 50], assuming the independence of the exceedances, the cumulative probability distribution  $F(\mathbf{u}, \zeta)$  follow the exponential member of the generalized Pareto distribution (GPD), that is:

$$F(\mathbf{u}, \zeta) \sim \exp\left[-\frac{\mathbf{u}(\zeta)}{\sigma(\zeta)}\right]. \quad (3)$$

The parameter  $\sigma(\zeta)$ , which is the scale parameter of the distribution, depends on the state  $\zeta$  in phase space and can be used to derive the local dimension via  $d(\zeta) = 1/\sigma(\zeta)$  [47]. In practice, the local dimension is computed by explicitly fitting an exponential distribution to the exceedances  $\mathbf{u}(\zeta)$ , see discussion in [51] and [52]. The estimate of the attractor's dimension derived from  $d(\zeta)$  seems to be more efficient than previous methods based on evaluating correlation integrals [53, 54]. The other local index, persistence ( $\theta^{-1}$ ), is defined as the inverse of the extremal index  $0 \leq \theta \leq 1$  [55, 56], a dimensionless parameter that measures the inverse of the length of clustering of extremes. In this context, extremes are defined as the *recurrences* within the neighborhood around a given state in phase space. Therefore, persistence ( $\theta^{-1}$ ) estimates the average number of consecutive recurrences, namely the time steps for the system to resemble a given state in its neighboring phase space.

Local dimension  $d$  and persistence  $\theta^{-1}$  have frequently been associated with the predictability of dynamical systems. More specifically, high local dimensions and low persistence are seen as an indication that the system is less predictable. The rationale for this is as follows. If a system requires more degrees of freedom to be described at a given point in the phase space, then its complexity is greater at that given point, making it possibly less predictable. Similarly, if a system leaves a neighborhood fast, then the dynamics of that neighbour is fast, and non-persistent; aspect that may indicate reduced predictability. While these arguments on predictability are qualitatively valid, and frequently correct, they approach predictability from a complexity ( $d$ ), and mean residence time ( $\theta^{-1}$ ) perspective, without directly addressing predictability.

In this work, we address the predictability of dynamical systems by building upon the framework of local dynamical indices just outlined. In particular, we introduce a new quantity named '*time-lag recurrence*' and denoted by  $\alpha_\eta$ . This new quantity uses neighboring states to monitor an ensemble of trajectories, and provides an indication in a statistical sense of the local predictability of dynamical systems. This is accomplished in a purely data-driven fashion, i.e. without requiring a model nor further simplifications on the data.

The computation of  $\alpha_\eta$  is based on the concept of recurrences introduced above, and measured via the logarithmic return quantity defined in equation (1). More specifically, using equation (2), we identify the set of states – i.e., recurrences –  $R_{t_\zeta}$  in the neighborhood of the reference state  $\zeta$  that have positive exceedance, that is:

$$R_{t_\zeta} = \{\mathbf{x}(t_{u_i}) : u_i(\zeta) > 0 \wedge |t_\zeta - t_{u_i}| > w\}_{i=1}^{N_n}, \quad (4)$$

where  $t_\zeta$  is the time that identifies the reference state  $\zeta$ ,  $w$  is the *Theiler window* [57] that excludes temporal neighbours of  $\zeta$ ,  $N_n$  is the number of exceedances (i.e., the number of temporally non-adjacent neighbors) at time  $t_\zeta$ ,  $t_{u_i}$  is the time corresponding to the exceedance  $u_i$ .

After having identified the *recurrences*  $R_{t_\zeta}$ , to characterise the local predictability of  $\zeta$  at time  $t_\zeta + \eta$  we first need to estimate how neighboring states evolve after time  $\eta$  has passed from  $t_\zeta$ . To this end, we first evolve the states within  $R_{t_\zeta}$  forward by time  $\eta$  (where  $\eta$  is also referred to as forecasting horizon), which leads to a set of new states, that we name *forward recurrences*

$$R_{t_\zeta}^\eta = \{\mathbf{x}(t + \eta) \mid \forall \mathbf{x}(t) \in R_{t_\zeta}\}. \quad (5)$$

These new states, that were evolved forward in time by  $\eta$  from time  $t_\zeta$ , are represented by the empty blue circles in Fig. 1, and are denoted by using the superscript  $(\cdot)^\eta$ .

Once we have defined the forward recurrences, equation (5), we need to define the *forward reference state*, that is: the reference state  $\zeta = \mathbf{x}(t_\zeta)$  after time  $\eta$ , and denoted by  $\zeta^\eta = \mathbf{x}(t_\zeta + \eta)$ . This forward reference state will have its own exceedances  $\mathbf{u}(\zeta^\eta)$  made of  $N_n$  elements  $\{u_i(\zeta^\eta)\}_{i=1}^{N_n}$ , and we can compute the *forward-reference-state recurrences*

$$R_{t_\zeta+\eta} = \{\mathbf{x}(t_{u_i}) : u_i(\zeta^\eta) > 0 \wedge |t_\zeta + \eta - t_{u_i}| > w\}_{i=1}^{N_n}, \quad (6)$$

in analogy to what was done for the reference state  $\zeta$  in equation (4).

With the three sets just introduced in equations (4–6), namely the recurrences  $R_{t_\zeta}$  in equation (4), the forward recurrences  $R_{t_\zeta}^\eta$  in equation (5), and the forward-reference-state recurrences  $R_{t_\zeta+\eta}$  in equation (6), we can define the *local predictability index* as follows:

$$\alpha_\eta(\zeta) = \frac{|R_{t_\zeta}^\eta \cap R_{t_\zeta+\eta}|}{|R_{t_\zeta}|} \quad (7)$$

where  $|\cdot|$  represents the number of elements within the set  $(\cdot)$ , and  $\cap$  is the intersection of two sets. Since both  $R_{t_\zeta}$  and  $R_{t_\zeta+\eta}$  are defined using the same quantile-based thresholds, the number of elements in one set is equal to the number of elements in the other set, that is:  $|R_{t_\zeta}| = |R_{t_\zeta+\eta}| = N_n$ . In addition, given that  $R_{t_\zeta}^\eta$  is defined from  $R_{t_\zeta}$ , the number of elements it contains is also equal to  $N_n$ . It follows that  $0 \leq \alpha_\eta(\mathbf{x}(t)) \leq 1$ . A value of  $\alpha_\eta(\zeta)$  close to 1 indicates high probability for a neighbor state to remain close to the reference state. We interpret this as a high predictability, in a statistical sense, for state  $\zeta$  at time  $t_\zeta$ , and forecasting horizon  $\eta$ , suggesting that most of its neighboring states stay close to the future trajectory of  $\zeta$  as time evolves. Conversely, when  $\alpha_\eta(\zeta)$  is close to zero, this implies that most of the initial neighbors have moved away from the trajectory of  $\zeta$  after time  $\eta$ , indicating low predictability in a statistical sense. The derivation of the new quantity  $\alpha_\eta(\zeta)$  relies on the quantile  $q$ , which is used to define recurrences, and on the distance function  $\text{dist}$ . The selection of the quantile  $q$  can be adapted for different application scenarios, and it reflects the local statistical predictability for different scales. This is not surprising as we are defining  $\alpha$  using extreme value theory where quantile choice is always an important step. In Supplementary Information Section B, we show an example of this scale-dependent behaviour using various  $q$ . This dependence on  $q$  can be seen as a favorable properties as it allows for analyzing predictability at different scales. Similarly, the selection of the distance function  $\text{dist}$  can be adapted depending on the application, noting that for physical systems, Euclidean distance has been shown to be an appropriate choice [47].

In addition, the new quantity  $\alpha_\eta(\zeta)$  is inherently connected to information theory, since estimating local predictability can be viewed as a process that quantifies the uncertainty or randomness within the system. In fact, if we take a conditional probability perspective, where  $P(A|B)$  represents the conditional probability of  $A$  given  $B$ , then we can reformulate the definition of  $\alpha_\eta$  in equation 7 as follows:

$$\alpha_\eta(\zeta) = P[\mathbf{x}(t + \eta) \in R_{t_\zeta+\eta} | \mathbf{x}(t) \in R_{t_\zeta}], \quad (8)$$

where  $A = \mathbf{x}(t + \eta) \in R_{t_\zeta+\eta}$  corresponds to recurrences of the reference state  $\zeta$  that, after being propagated forward in time by  $\eta$ , belong to the forward-state neighborhood  $\zeta^\eta$  (i.e., they are forward-reference-state recurrences), and  $B = \mathbf{x}(t) \in R_{t_\zeta}$  corresponds to the recurrences of the reference state  $\zeta$ .

The new predictability index has a number of advantages compared to existing predictability measures: (i) it is purely data-driven, (ii) it is local as it measures instantaneous properties, (iii) it does not require simplifications to be made on the data, and (iv) it is suitable for high dimensional datasets.

However, given that it uses future states, it cannot be readily used for real-time predictability analyses, for instance in the context of operational weather forecasting. We shall discuss this aspect in a later section and propose a practical way to address this limitation.

It is helpful here to emphasize some key differences to other data-driven ways of measuring local predictability properties. The classical algorithms proposed in [58] to measure the Lyapunov exponents from available time series

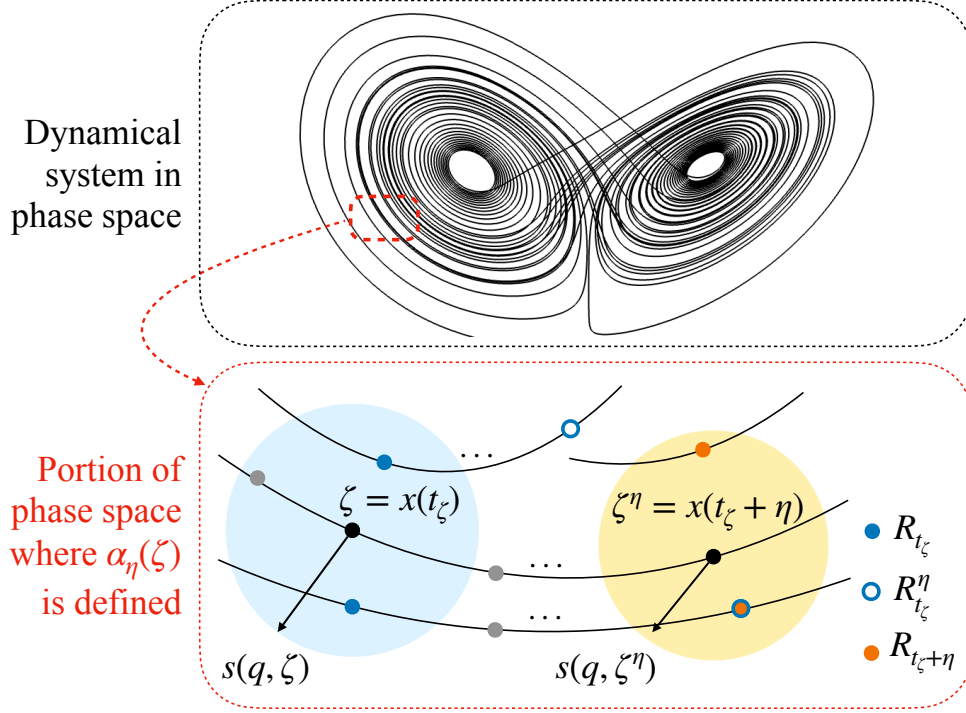


Figure 1: Schematic illustration of the computation of  $\alpha_\eta(t)$ .

allow to estimate the growth rate of the  $n$ -dimensional volumes (for  $n$  smaller than or equal to the dimension of the phase space) defined by  $n + 1$  initially nearby points. The strategy there strongly relies on using delay coordinates in order to take advantage of Takens' theorem [59] and reconstruct the key properties of the attractor. By selecting nearby points belonging to a region of interest, local properties can be extracted. Following such geometrical construction, one obtains that

$$P[\text{dist}(\mathbf{x}(t + \eta), \zeta^\eta) < \epsilon | \text{dist}(\mathbf{x}(t), \zeta) < \epsilon] \approx e^{-(\sum_{\lambda_j > 0} \lambda_j^\zeta) \eta}. \quad (9)$$

where the exponent is proportional to sum of positive local, finite-time Lyapunov exponents. Clearly  $\epsilon$  has to be small. After comparing Eqs. 8 and 9 it is tempting to deduce  $\alpha_\eta \approx e^{-(\sum_{\lambda_j > 0} \lambda_j^\zeta) \eta}$  (see later discussion on specific numerical examples). Yet, a key difference between the two definitions exist when one applied them to actual data, because in Eq. 8 one considers neighbourhoods of  $\zeta$  and  $\zeta^\eta$  having the same number of points (thanks to the use of quantiles in defining the threshold of the distance observables), so that such neighbourhoods will in general have a different radius (which is instead identical and equal to  $\epsilon$  in Eq. 9).

## Results and discussion

We have computed the new metric  $\alpha_\eta(\zeta)$  for both idealized and real-world dynamical systems of varying complexity, including the Lorenz-63 attractor and atmospheric circulation patterns. These results are reported in the following subsections. Additionally, in the Supplementary Information, we provide several supplementary results for other systems. Following the discussion of results obtained from various systems, we propose a method for utilizing this index in real-time, addressing the issue introduced at the end of the previous section.

### Idealized dynamical systems

We consider the Lorenz-63 attractor as an example of idealized dynamical system. The data for this test case is obtained from the numerical simulation of the Lorenz-63 system, with a time resolution of  $5 \times 10^{-3}$  over  $1 \times 10^5$  time steps, using the classical set of parameters that leads the system to be chaotic (for further details see Supplementary Information Section A). Figure 2 shows the distribution of  $\alpha_\eta$  for the Lorenz-63 system, for five different forecasting horizons:  $\eta = [0.05, 0.1, 0.2, 1, 2] \eta_\ell$ . The quantity  $\eta_\ell$ , that represents the Lyapunov time, is equal to 1.1 time units and is computed as the inverse of the maximum Lyapunov exponent of the Lorenz-63 system.

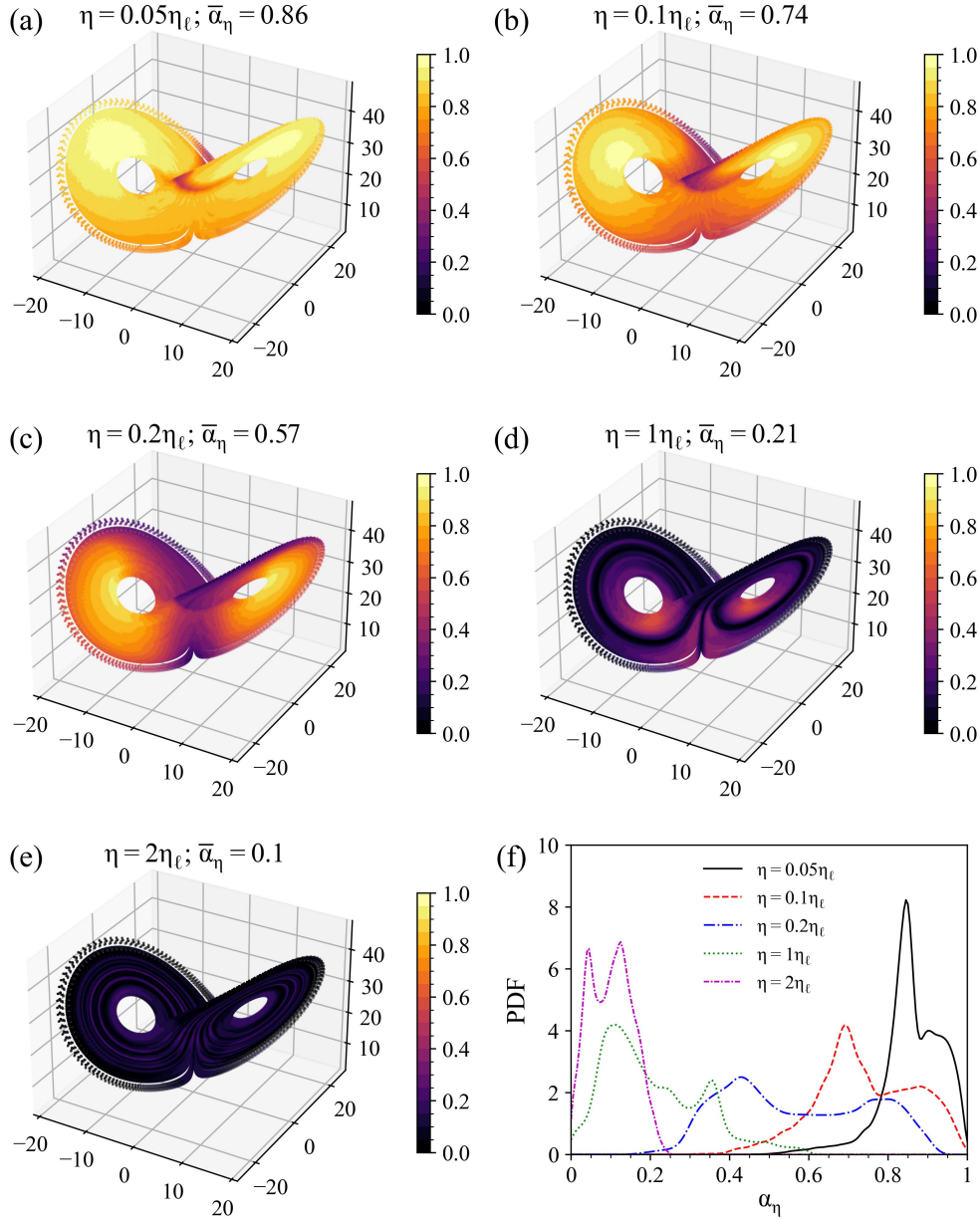


Figure 2: Distribution of  $\alpha_\eta$  at different prediction horizons for the Lorenz-63 system. (a-e) Lorenz attractor colored by  $\alpha_\eta$  values at five different forecasting horizons:  $\eta = [0.05, 0.1, 0.2, 1, 2]\eta_\ell$ , each corresponding to timesteps:  $L = [11, 22, 44, 220, 440]$ . (f) Probability distribution of  $\alpha_\eta$  at the same five different forecasting horizons.

Figs. 2(a-e) depict the Lorenz attractor in the phase space colored by the values of  $\alpha_\eta$ , for the 5 different forecasting horizons considered. For each panel in Fig. 2(a-e), the title on the top reports the forecasting horizon, and the average of the local predictability, namely  $\bar{\alpha}_\eta$ . We note how, as we increase the forecasting horizon,  $\bar{\alpha}_\eta$  tends to decrease, as also depicted by the increasingly darker colors from Fig. 2(a) to Fig. 2(e). This result is in agreement with what we shall expect – the longer the forecasting horizon, the less predictable the system. This conclusion is also summarized in Fig. 2(f), that shows the distribution of  $\alpha_\eta$  for the five different forecasting horizons: the two longest horizons display a distribution peaked on low values of predictability ( $<0.2$ ), while shorter horizons tend to display distributions peaked toward higher values of predictability.

These results confirm that the predictability of the Lorenz-63 system is closely related to the local reference state in the phase space and the forecasting horizon. In addition, the phase-space distribution of  $\alpha_\eta$  shows some interesting features,

namely: for short forecasting horizons the region where the Lorenz-63 attractor switches lobes seem to have low predictability (Fig. 2(a)), while for longer forecasting horizons, also the wings of the attractor become less predictable (Fig. 2(b,c)). These findings are consistent with previous studies on local predictability of Lorenz systems [27, 21]. Remarkably, for forecasting horizons twice the Lyapunov time, the overall system loses predictability (Fig. 2(e)).

To further show how  $\alpha_\eta$  reveals phase-space and time features that can be used for understanding the predictability of dynamical systems, we present the evolution of the average  $\alpha_\eta$  for seven different clusters (or regions) of the Lorenz-63 attractor. These clusters are depicted in Fig. 3, and are obtained by applying a K-means clustering method to the Lorenz-63 data used for Fig. 2, similar to the one adopted in [60]. Interestingly, the clustering identifies portions of the attractor in the phase space that seem to match some of the observations made for Fig. 2. In particular, cluster 4 represents the region where trajectories are switching lobes, clusters 1, 2, 6, and 7 represent the wings of the attractor, while clusters 3 and 5 represent intermediate regions that contain features from the five clusters just described. We note how, as expected, cluster 4 has the lowest short-term predictability among the regions considered, with a sudden drop at short forecasting horizons (yellow line). The wings of the attractor follow, with clusters 2 (dark orange) and 6 (green) being the least predictable after cluster 4, immediately followed by clusters 1 (red) and 7 (blue). Clusters 3 and 5, after a sudden predictability drop similar to the one experienced for cluster 4, maintain relatively good predictability for larger forecasting horizons compared to all other clusters. This is confirmed, if we look at the area under each curve (AUC) reported in Figure 3, that represent the average predictability of each cluster with respect to the forecasting horizons, with clusters 3 and 5 having the highest average predictability, and cluster 4 the lowest.

We also note that, despite the general trend of predictability decreasing as the prediction horizon increases, it is interesting to note that  $\alpha_\eta$  does not always decrease monotonically. There are instances showing returns of predictability, as also reported in [61], and as reflected more clearly in Fig. 3(b); see also discussion above regarding the relationship between the definitions provided in Eqs. 8 and 9.

Other than the Lorenz system, results for other idealized dynamical systems are also presented to assess the behavior of our local predictability index in notable cases. In particular, we consider the chaotic Rössler system, and the stochastic spring-slider system introduced in [16] to describe laboratory and slow earthquakes (Supplementary Information Section C). The results for all these additional systems are as expected. For the Rössler system, we obtain a similar behavior as the Lorenz-63 system. For the stochastic spring-slider system, we obtain a relatively low predictability, that is expected given the stochastic nature of the system. We note that the results included in the Supplementary Information is representative of several additional test cases that were performed as part of this study, and that can be found in the repository containing the code for the local predictability index that is provided as part of this study.

We additionally compare our results with the nonlinear local Lyapunov exponent (NLLE) [36, 37], an established index used to quantify local predictability that we find closely relevant, as reported in Supplementary Information Section D. The results for the NLLE display some notable differences with our local predictability index while also showing some similarities. These differences are arguably due to the use of different perspectives in defining predictability. Their framework stems from the Lyapunov exponent, focusing on the exponential error growth rate, while our method is rooted in the concept of *recurrences* in dynamical system theory. We acknowledge that both methods have their own caveats: NLLE predefines the rule of error growth, while our method neglects the information on trajectories that have left the neighborhood. To overcome this, we propose an extension of our predictability index by accounting for the information given by the distances of all the neighboring trajectories – i.e., both those that remained close to the reference state and those that departed from it, as shown in Supplementary Information Section E.

Furthermore, we have compared  $\alpha_\eta$  with the previously introduced local dynamical indices. This allows us to directly compare the relationship between predictability and local dynamical properties, rather than relying solely on prior assumptions. In Figure 4, we show scatter plots of the local predictability index versus the local dimension  $d$  and the persistence  $\theta^{-1}$ . We note that the intuition that high dimension and low persistence means low predictability does not hold for the case of the Lorenz-63 system. Specifically, states on the two wings of the Lorenz attractor exhibit low persistence (high values of  $\theta$ ), indicating that these states are likely to leave the neighborhood immediately [62]. However, they also demonstrate high predictability over short forecasting horizons. This is not surprising when considering the dynamics on the wings of the Lorenz attractor—although these states may leave the neighborhood quickly, their neighboring trajectories do not diverge significantly, making them predictable in short forecasting horizons.

We show, in the next section, that for the real-world data considered, the agreement between the interpretation of the  $d$ - $\theta$  space and  $\alpha_\eta$  seems to hold instead.

## Climate Data

In addition to the test cases presented for idealized systems, we computed  $\alpha_\eta$  using real-world data. In particular, focused on studying the predictability of large-scale atmospheric circulation patterns in the Europe-Atlantic sector

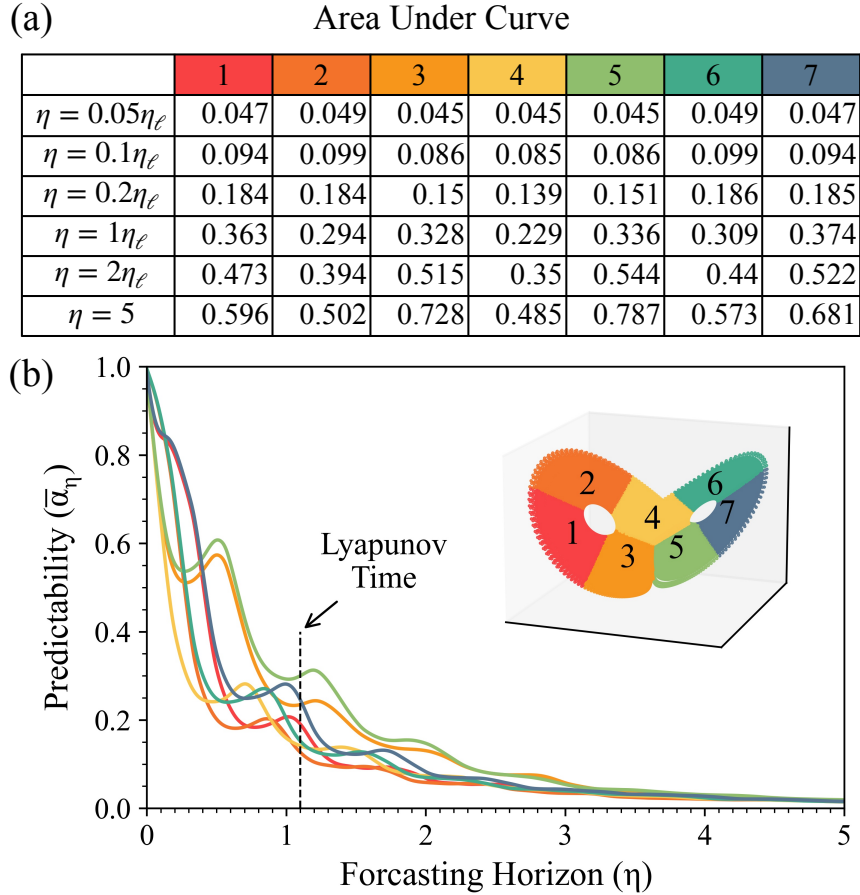


Figure 3: Temporal and phase-spatial variations of  $\alpha_\eta$ . The evolution of  $\alpha_\eta$  averaged across seven clusters of states on the Lorenz-63 attractor. Inset: Lorenz-63 attractor colored to represent seven clusters obtained from K-means algorithm, each labeled with corresponding numbers.

(80°W to 50°E, 22.5°N to 70°N), using state-of-the-art ERA5 reanalysis data [63] from 1979 to 2022, with a spatial resolution of 0.25°. We selected the daily mean 500 hPa geopotential height (Z500) as the representative variable, which has been frequently used to characterize circulation dynamics in the mid-latitudes [64, 65, 66, 67, 68]. This means that we consider the Z500 map for each day as a state along the system’s trajectory in phase space.

Specifically, in the Euro-Atlantic sector, the definition of weather regimes offers a direct way of classifying atmospheric states. Weather regimes are defined as recurrent and quasi-stationary large-scale circulation patterns [69, 68]. Despite being a coarse characterization of atmospheric variability, weather regimes are found to be associated with conditions that are specifically favorable for certain types of weather extremes [70], and they have exhibited varying levels of predictability in real-time forecasting [71]. In this work, we have adopted the four-regime definition widely used for scientific research [72], although various definitions for weather regimes exist [72, 73]. All extended wintertime (DJFM) Z500 patterns are classified into five different categories including NAO+, Alantic Ridge (AR), NAO-, Scandinavian Blocking (SB) and no regime, using a method slightly adapted from [74] (see Supplementary Information Section E for details).

Figure 5 shows the distribution of  $\alpha_\eta$  across all five categories for  $\eta = 1 - 3$  days. The results indicate that the NAO- regime has the highest predictability, followed by NAO+, with the remaining two regimes showing no significant difference from having no regime for  $\eta = 1$  day. For  $\eta = 2$  and 3 days, NAO+ and NAO- still maintain notably higher mean values compared to other categories, with the no regime category having the lowest values, confirming that large scale weather regimes are a primary source of predictability in the Euro-Atlantic region. These results are in excellent agreement with previous investigation dedicated to the Euro-Atlantic sector: NAO- exhibits stronger predictability than other regimes, while the blocked zonal regimes (SB and AR) are notoriously unpredictable [71, 62] [75, Section

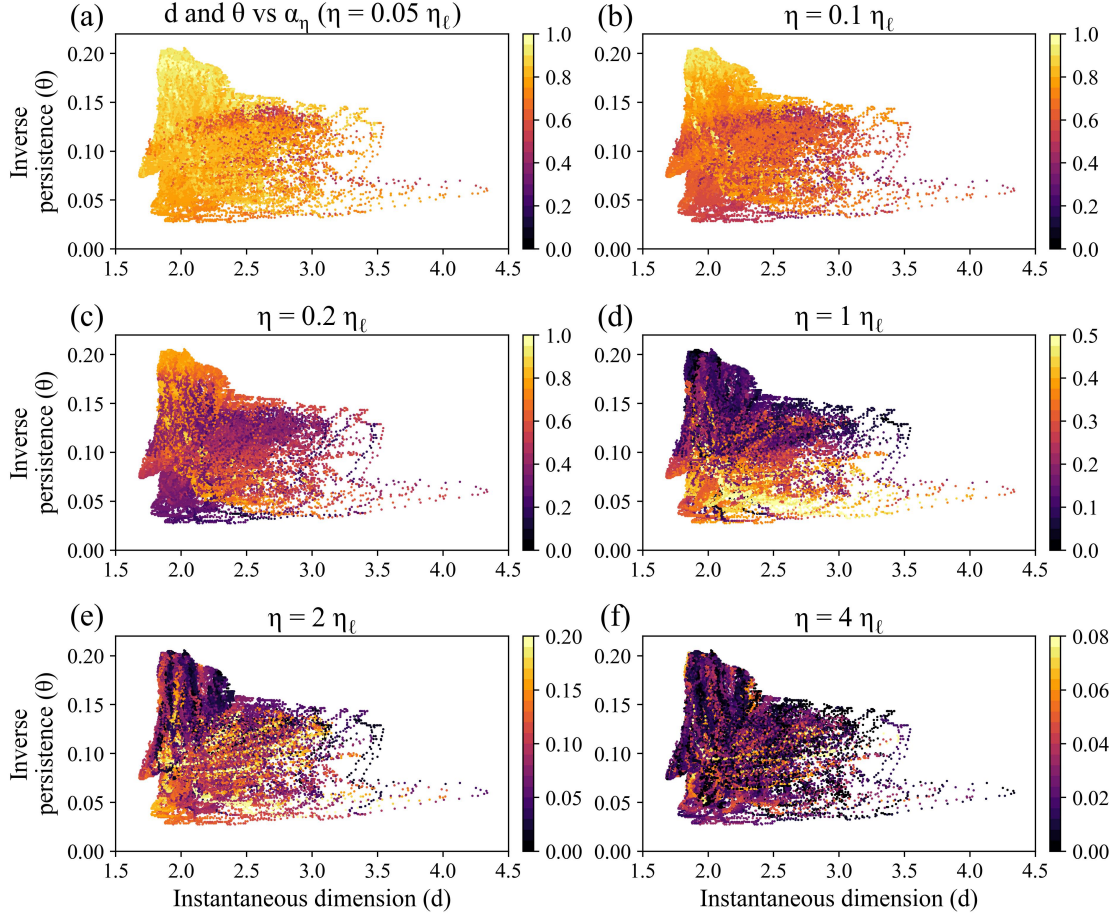


Figure 4: Comparative analysis of  $\alpha_\eta$  with local dynamical indices for the Lorenz-63 system. (a-f) Scatter plots of local dimension versus local inverse persistence, where each dot represents one state. All states are colored based on  $\alpha_\eta$  values for  $\eta = [0.05, 0.1, 0.2, 1, 2, 4]\eta_\ell$ . Note that the color scale is different in the last three panels in order to improve readability.

8.2.2]). Additionally, we find further confirmation of the general fact that blockings are associated with anomalously high instability compared to zonal flow conditions [76, 77].

These findings further validate the effectiveness of our index, supported by both the underlying physical explanations and the model-based prediction results. Here we stress that we applied this index to the Euro-Atlantic region because it is an ideal test bed with well-established relevant research; however, this index can be extended to any other variables and domains.

Fig. 6 illustrates scatter plots of local dimension  $d$  vs inverse persistence  $\theta$  for all the atmospheric states, colored by the predictability index  $\alpha_\eta$ , for different prediction horizons ( $\eta$ ) ranging from 1 to 4 days. The overall predictability drops as  $\eta$  increases, as expected due to the highly chaotic nature of atmospheric circulation. Notably, states in the lower-left corner of the  $d$ - $\theta$  scatter plot space consistently exhibit higher-than-average predictability, regardless of the value of  $\eta$ . This aligns with the assumption in previous works for which states with low local dimension and high persistence are most predictable. From the dynamical system theory perspective, a lower local dimension indicates a simpler dynamics, while higher persistence means that a state is likely to remain similar to its current configuration for a longer time. This result confirms our previous hypothesis while also further demonstrating the effectiveness of the proposed predictability index for high-dimensional systems.

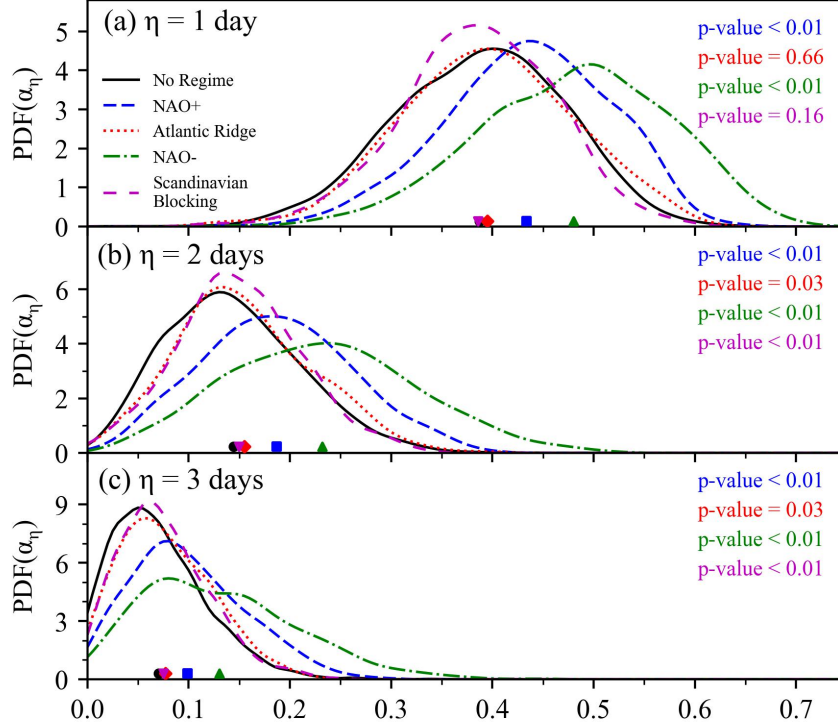


Figure 5: Predictability analysis of North Atlantic wintertime weather regimes. (a-c) Probability distribution of  $\alpha_\eta$  for four weather regime and no regime: NAO+ (blue dashed line), Atlantic Ridge (red dotted line), NAO- (green dot-dashed line), Scandinavian Blocking (magenta loosely dashed line), and no regime (black line), for  $\eta = 1 - 3$  days. The markers on the x-axis show the mean value of  $\alpha_\eta$  for different categories. The statistical significance is evaluated between the distribution of each weather regime and that of no regime using the Kolmogorov-Smirnov test.

### A note on real-time predictability

Our findings demonstrate the agreement of  $\alpha_\eta$  with known results, positioning it as a viable index for analysing the local predictability of dynamical systems. Yet, one key point remains outstanding:  $\alpha_\eta$ , as is, cannot be used for real-time applications, as it requires the future state of the system. However, since  $\alpha_\eta$  quantifies local predictability information in the phase space, for a given unprecedented state  $\zeta'$ , we can compute the average  $\alpha_\eta$  of its analogues (i.e., similar states to  $\zeta'$  that appeared in the past). The number of analogues can be set once again using a quantile threshold, but this could be different from the one used to define the local properties. In practice, if we consider  $N_a$  analogues, indicated by  $\{\mathbf{x}(t_{a_i})\}_{i=1}^{N_a}$ , with  $t_{a_i}$  being the time at which the analogue number  $a_i$  occurred, the predictability index proxy is:

$$\hat{\alpha}_\eta(\zeta') = \frac{1}{N_a} \sum_{i=1}^{N_a} \alpha_\eta(\mathbf{x}(t_{a_i})) \quad (10)$$

This can be used for real-time predictability analyses of dynamical systems. For instance, in the context of weather and climate applications, we can identify the analogues of today's data, and compute the predictability index proxy  $\hat{\alpha}_\eta(\zeta')$  using equation 10. This will give us the real-time predictability of the system as of today, thereby allowing us to adopt the index for real-time applications. An example of real-time applications is presented in Supplementary Information Section E, where we show an application for the Lorenz-63 system, with the real-time predictability proxy  $\hat{\alpha}_\eta(\zeta')$  successfully capturing the phase-space and time features of the predictability for the Lorenz-63 system.

## Conclusions

This work complements the rich body of work on the pivotal topic of predictability of dynamical systems, from the pioneering works of Poincaré and Lorenz, to modern dynamical system theory and its applications to real-life complex systems, especially in the context and weather and climate prediction. In particular, we provide a new index that can infer

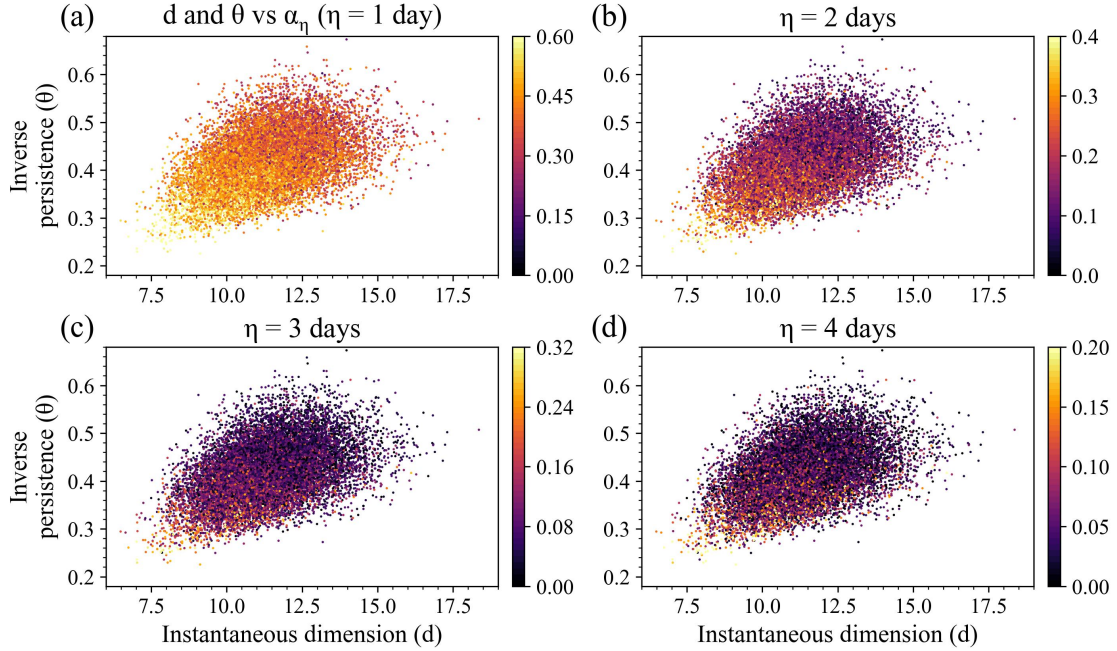


Figure 6: Comparative analysis of  $\alpha_\eta$  with local dynamical indices for Z500 patterns in the Europe-Atlantic sector. (a-d) Scatter plots of local dimension versus local inverse persistence, where each dot represents one daily Z500 pattern. All states are colored based on  $\alpha_\eta$  values for  $\eta = 1 - 4$  days. Note that the color scale is different in each panel in order to improve readability.

state-dependent predictability from high-dimensional observational datasets, overcoming the curse of dimensionality that affects more traditional approaches. While our approach has a resemblance with classical data-driven methods used for performing Lyapunov analysis on general systems [58, 78], the local predictability index is indeed novel and is able to describe flexibly key dynamical features of complex systems. We applied this index to dynamical systems of varying complexity, ranging from idealized low-dimensional systems to real-world high-dimensional atmospheric reanalysis datasets and we showcased its effectiveness. In particular, our findings confirm that when in the Euro-Atlantic sector of the mid-latitudes a blocking is present, the predictability of the atmosphere is typically anomalously low. We further showed how the new index reveals the scale-dependent nature of predictability by using different quantiles, and how it can be used in real-time problems. Our approach also addresses the ambiguity in terms of predictability that surrounds the two local dynamical indices, namely dimension  $d$  and persistence  $\theta^{-1}$ , providing a framework that directly addresses predictability.

We conclude this work with a note. The definition of  $\alpha_\eta$ , does not require  $\eta > 0$ . Therefore,  $\alpha_\eta$  can be computed backward in time using  $\eta < 0$ . In this case,  $\alpha_\eta$  characterizes the dynamics of the system as it approaches the reference state of interest, and it provides information that are entirely different from the forward-in-time analysis presented so far, using  $\eta > 0$ . Indeed, the backward predictability analysis can be used for understanding the dynamical pathways leading to extreme events as well as other phenomena in dynamical systems [79, 80].

## Acknowledgments

G.M. acknowledges support from MOE Tier 2 grant no 22-5191-A0001-0, titled: ‘Prediction-to-Mitigation with Digital Twins of the Earth’s Weather’. V.L. acknowledges the support provided by the Horizon Europe Project ClimTIP (Grant No. 100018693) and by the EPSRC project LINK (Grant No. EP/Y026675/1).

## References

- [1] Isaac Newton. *Philosophiæ naturalis principia mathematica*, volume 1. G. Brookman, 1833.
- [2] Henri Poincaré. Sur le problème des trois corps et les équations de la dynamique. *Acta mathematica*, 13(1):A3–A270, 1890.

- [3] Steven H Strogatz. *Nonlinear dynamics and chaos: with applications to physics, biology, chemistry, and engineering*. CRC press, 2018.
- [4] J-P Eckmann and David Ruelle. Ergodic theory of chaos and strange attractors. *Reviews of modern physics*, 57(3):617, 1985.
- [5] A. Pikovsky and A. Politi. *Lyapunov Exponents: A Tool to Explore Complex Dynamics*. Cambridge University Press, 2016.
- [6] H. Risken and T. Frank. *The Fokker-Planck Equation: Methods of Solution and Applications*. Springer Series in Synergetics. Springer Berlin Heidelberg, 2012.
- [7] G.A. Pavliotis. *Stochastic Processes and Applications: Diffusion Processes, the Fokker-Planck and Langevin Equations*. Texts in Applied Mathematics. Springer New York, 2014.
- [8] K. Hasselmann. Stochastic climate models Part I. Theory. *Tellus*, 28(6):473–485, 1976.
- [9] Valerio Lucarini and Mickaël D. Chekroun. Theoretical tools for understanding the climate crisis from hasselmann’s programme and beyond. *Nature Reviews Physics*, 2023.
- [10] H. Mori. Transport, Collective Motion, and Brownian Motion. *Progress of Theoretical Physics*, 33(3):423–455, mar 1965.
- [11] Robert Zwanzig. Memory effects in irreversible thermodynamics. *Physical Review*, 124(4):983–992, 1961.
- [12] M. Santos Gutiérrez, V. Lucarini, M. D. Chekroun, and M. Ghil. Reduced-order models for coupled dynamical systems: Data-driven methods and the Koopman operator. *Chaos*, 31(5):053116, 2021.
- [13] Cécile Penland and Theresa Magorian. Prediction of niño 3 sea surface temperatures using linear inverse modeling. *Journal of Climate*, 6(6):1067 – 1076, 1993.
- [14] D. Kondrashov, S. Kravtsov, and M. Ghil. Empirical mode reduction in a model of extratropical low-frequency variability. *Journal of the Atmospheric Sciences*, 63(7):1859 – 1877, 2006.
- [15] Davide Faranda, Yuzuru Sato, Brice Saint-Michel, Cecile Wiertel, Vincent Padilla, Bérengère Dubrulle, and François Daviaud. Stochastic chaos in a turbulent swirling flow. *Physical review letters*, 119(1):014502, 2017.
- [16] Adriano Gualandi, Davide Faranda, Chris Marone, Massimo Cocco, and Gianmarco Mengaldo. Deterministic and stochastic chaos characterize laboratory earthquakes. *Earth and Planetary Science Letters*, 604:117995, 2023.
- [17] SK Nath, A Raj, KKS Thingbaijam, and A Kumar. Ground motion synthesis and seismic scenario in guwahati city—a stochastic approach. *Seismological Research Letters*, 80(2):233–242, 2009.
- [18] L. T. Giorgini, W. Moon, N. Chen, and J. S. Wettlaufer. Non-gaussian stochastic dynamical model for the el niño southern oscillation. *Phys. Rev. Res.*, 4:L022065, Jun 2022.
- [19] Edward N Lorenz. Deterministic nonperiodic flow. *Journal of atmospheric sciences*, 20(2):130–141, 1963.
- [20] Stefan Siegert and Holger Kantz. Prediction of complex dynamics: who cares about chaos? *Chaos Detection and Predictability*, pages 249–269, 2016.
- [21] Timothy N Palmer. Extended-range atmospheric prediction and the lorenz model. *Bulletin of the American Meteorological Society*, 74(1):49–66, 1993.
- [22] Hans Crauel, Arnaud Debussche, and Franco Flandoli. Random attractors. *Journal of Dynamics and Differential Equations*, 9:307–341, 1997.
- [23] Guido Boffetta, Massimo Cencini, Massimo Falcioni, and Angelo Vulpiani. Predictability: a way to characterize complexity. *Physics reports*, 356(6):367–474, 2002.
- [24] Ulrich Parlitz. Estimating lyapunov exponents from time series. *Chaos detection and predictability*, pages 1–34, 2016.
- [25] Valery Iustinovich Oseledec. A multiplicative ergodic theorem, lyapunov characteristic numbers for dynamical systems. *Transactions of the Moscow Mathematical Society*, 19:197–231, 1968.
- [26] Chiara Cecilia Maiocchi, Valerio Lucarini, Andrey Gritsun, and Yuzuru Sato. Heterogeneity of the attractor of the lorenz ’96 model: Lyapunov analysis, unstable periodic orbits, and shadowing properties. *Physica D: Nonlinear Phenomena*, 457:133970, 2024.
- [27] Jon M Nese. Quantifying local predictability in phase space. *Physica D: Nonlinear Phenomena*, 35(1-2):237–250, 1989.
- [28] Christine Ziehmann, Leonard A Smith, and Jürgen Kurths. Localized lyapunov exponents and the prediction of predictability. *Physics Letters A*, 271(4):237–251, 2000.

- [29] Julia Slingo and Tim Palmer. Uncertainty in weather and climate prediction. *Philosophical Transactions of the Royal Society A: Mathematical, Physical and Engineering Sciences*, 369(1956):4751–4767, 2011.
- [30] Alberto Carrassi, Marc Bocquet, Laurent Bertino, and Geir Evensen. Data assimilation in the geosciences: An overview of methods, issues, and perspectives. *Wiley Interdisciplinary Reviews: Climate Change*, 9(5), 2018. Cited by: 355; All Open Access, Bronze Open Access, Green Open Access.
- [31] Henry DI Abarbanel, Reggie Brown, and Matthew B Kennel. Variation of lyapunov exponents on a strange attractor. *Journal of Nonlinear Science*, 1:175–199, 1991.
- [32] Bruno Eckhardt and Demin Yao. Local lyapunov exponents in chaotic systems. *Physica D: Nonlinear Phenomena*, 65(1-2):100–108, 1993.
- [33] Massimo Cencini and Angelo Vulpiani. Finite size lyapunov exponent: review on applications. *Journal of Physics A: Mathematical and Theoretical*, 46(25):254019, jun 2013.
- [34] E Aurell, Guido Boffetta, Andrea Crisanti, G Paladin, and Angelo Vulpiani. Predictability in the large: an extension of the concept of lyapunov exponent. *Journal of physics A: Mathematical and general*, 30(1):1, 1997.
- [35] Guido Boffetta, P Giuliani, G Paladin, and A Vulpiani. An extension of the lyapunov analysis for the predictability problem. *Journal of the Atmospheric Sciences*, 55(23):3409–3416, 1998.
- [36] Ruiqiang Ding and Jianping Li. Nonlinear finite-time lyapunov exponent and predictability. *Physics Letters A*, 364(5):396–400, 2007.
- [37] Xiao-Wei HUAI, Jian-Ping LI, Rui-Qiang DING, Jie FENG, and De-Qiang LIU. Quantifying local predictability of the lorenz system using the nonlinear local lyapunov exponent. *Atmospheric and Oceanic Science Letters*, 10(5):372–378, 2017.
- [38] Karlheinz Geist, Ulrich Parlitz, and Werner Lauterborn. Comparison of different methods for computing lyapunov exponents. *Progress of theoretical physics*, 83(5):875–893, 1990.
- [39] Timothy DelSole and Michael K Tippett. Predictability: Recent insights from information theory. *Reviews of Geophysics*, 45(4), 2007.
- [40] Tapio Schneider and Stephen M Griffies. A conceptual framework for predictability studies. *Journal of climate*, 12(10):3133–3155, 1999.
- [41] Richard Kleeman. Statistical predictability in the atmosphere and other dynamical systems. *Physica D: Nonlinear Phenomena*, 230(1-2):65–71, 2007.
- [42] Lai-Yung Leung and Gerald R North. Information theory and climate prediction. *Journal of Climate*, 3(1):5–14, 1990.
- [43] Richard Kleeman. Measuring dynamical prediction utility using relative entropy. *Journal of the atmospheric sciences*, 59(13):2057–2072, 2002.
- [44] Xiaoli Li, Gaoxian Ouyang, and Douglas A Richards. Predictability analysis of absence seizures with permutation entropy. *Epilepsy research*, 77(1):70–74, 2007.
- [45] Olawale J Ikuyajolu, Fabrizio Falasca, and Annalisa Bracco. Information entropy as quantifier of potential predictability in the tropical indo-pacific basin. *Frontiers in Climate*, 3:675840, 2021.
- [46] Christoph Bandt and Bernd Pompe. Permutation entropy: a natural complexity measure for time series. *Physical review letters*, 88(17):174102, 2002.
- [47] Valerio Lucarini, Davide Faranda, Jorge Miguel Milhazes de Freitas, Mark Holland, Tobias Kuna, Matthew Nicol, Mike Todd, Sandro Vaienti, et al. *Extremes and recurrence in dynamical systems*. John Wiley & Sons, 2016.
- [48] Ronald Aylmer Fisher and Leonard Henry Caleb Tippett. Limiting forms of the frequency distribution of the largest or smallest member of a sample. In *Mathematical proceedings of the Cambridge philosophical society*, volume 24, pages 180–190. Cambridge University Press, 1928.
- [49] Ana Cristina Moreira Freitas, Jorge Milhazes Freitas, and Mike Todd. Hitting time statistics and extreme value theory. *Probability Theory and Related Fields*, 147(3):675–710, 2010.
- [50] Valerio Lucarini, Davide Faranda, and Jeroen Wouters. Universal behaviour of extreme value statistics for selected observables of dynamical systems. *Journal of statistical physics*, 147:63–73, 2012.
- [51] George Datsleris, Inga Kottlarz, Anton P Braun, and Ulrich Parlitz. Estimating fractal dimensions: A comparative review and open source implementations. *Chaos: An Interdisciplinary Journal of Nonlinear Science*, 33(10), 2023.

- [52] Flavio Pons, Gabriele Messori, and Davide Faranda. Statistical performance of local attractor dimension estimators in non-axiom a dynamical systems. *Chaos: An Interdisciplinary Journal of Nonlinear Science*, 33(7), 2023.
- [53] Peter Grassberger and Itamar Procaccia. Characterization of strange attractors. *Phys. Rev. Lett.*, 50:346–349, Jan 1983.
- [54] Mingzhou Ding, Celso Grebogi, Edward Ott, Tim Sauer, and James A. Yorke. Estimating correlation dimension from a chaotic time series: when does plateau onset occur? *Physica D: Nonlinear Phenomena*, 69(3):404–424, 1993.
- [55] Ana Cristina Moreira Freitas, Jorge Milhazes Freitas, and Mike Todd. The extremal index, hitting time statistics and periodicity. *Advances in Mathematics*, 231(5):2626–2665, 2012.
- [56] Nicholas R Moloney, Davide Faranda, and Yuzuru Sato. An overview of the extremal index. *Chaos: An Interdisciplinary Journal of Nonlinear Science*, 29(2), 2019.
- [57] James Theiler. Spurious dimension from correlation algorithms applied to limited time-series data. *Physical review A*, 34(3):2427, 1986.
- [58] Alan Wolf, Jack B. Swift, Harry L. Swinney, and John A. Vastano. Determining lyapunov exponents from a time series. *Physica D: Nonlinear Phenomena*, 16(3):285–317, 1985.
- [59] Floris Takens. Detecting strange attractors in turbulence. In David Rand and Lai-Sang Young, editors, *Dynamical Systems and Turbulence, Warwick 1980*, pages 366–381, Berlin, Heidelberg, 1981. Springer Berlin Heidelberg.
- [60] Eurika Kaiser, Bernd R Noack, Laurent Cordier, Andreas Spohn, Marc Segond, Markus Abel, Guillaume Daviller, Jan Östh, Siniša Krajnović, and Robert K Niven. Cluster-based reduced-order modelling of a mixing layer. *Journal of Fluid Mechanics*, 754:365–414, 2014.
- [61] Leonard A Smith, C Ziehmann, and K Fraedrich. Uncertainty dynamics and predictability in chaotic systems. *Quarterly Journal of the Royal Meteorological Society*, 125(560):2855–2886, 1999.
- [62] Davide Faranda, Gabriele Messori, and Pascal Yiou. Dynamical proxies of north atlantic predictability and extremes. *Scientific reports*, 7(1):41278, 2017.
- [63] Hans Hersbach, Bill Bell, Paul Berrisford, Shoji Hirahara, András Horányi, Joaquín Muñoz-Sabater, Julien Nicolas, Carole Peubey, Raluca Radu, Dinand Schepers, et al. The era5 global reanalysis. *Quarterly Journal of the Royal Meteorological Society*, 146(730):1999–2049, 2020.
- [64] R. Benzi, P Malguzzi, A. Speranza, and A. Sutera. The statistical properties of general atmospheric circulation: Observational evidence and a minimal theory of bimodality. *Quarterly Journal of the Royal Meteorological Society*, 112(473):661–674, 1986.
- [65] Kingtse Mo and Michael Ghil. Cluster analysis of multiple planetary flow regimes. *Journal of Geophysical Research: Atmospheres*, 93(D9):10927–10952, 1988.
- [66] Alessandro Dell’Aquila, Valerio Lucarini, Paolo M. Ruti, and Sandro Calmanti. Hayashi spectra of the northern hemisphere mid-latitude atmospheric variability in the ncep–ncar and ecmwf reanalyses. *Climate Dynamics*, 25(6):639–652, Nov 2005.
- [67] Aglaé Jézéquel, Pascal Yiou, and Sabine Radanovics. Role of circulation in european heatwaves using flow analogues. *Climate dynamics*, 50(3):1145–1159, 2018.
- [68] Sebastian Springer, Alessandro Laio, Vera Melinda Galfi, and Valerio Lucarini. Unsupervised detection of large-scale weather patterns in the northern hemisphere via markov state modelling: from blockings to teleconnections. *npj Climate and Atmospheric Science*, 7(1):105, 2024.
- [69] Paul-Antoine Michelangeli, Robert Vautard, and Bernard Legras. Weather regimes: Recurrence and quasi stationarity. *Journal of the atmospheric sciences*, 52(8):1237–1256, 1995.
- [70] P Yiou and M Nogaj. Extreme climatic events and weather regimes over the north atlantic: when and where? *Geophysical Research Letters*, 31(7), 2004.
- [71] Laura Ferranti, Susanna Corti, and Martin Janousek. Flow-dependent verification of the ecmwf ensemble over the euro-atlantic sector. *Quarterly Journal of the Royal Meteorological Society*, 141(688):916–924, 2015.
- [72] Robert Vautard. Multiple weather regimes over the north atlantic: Analysis of precursors and successors. *Monthly weather review*, 118(10):2056–2081, 1990.
- [73] Christian M Grams, Remo Beerli, Stefan Pfenninger, Iain Staffell, and Heini Wernli. Balancing europe’s wind-power output through spatial deployment informed by weather regimes. *Nature climate change*, 7(8):557–562, 2017.

- [74] Christophe Cassou. Intraseasonal interaction between the madden–julian oscillation and the north atlantic oscillation. *Nature*, 455(7212):523–527, 2008.
- [75] R Owens and Tim Hewson. *ECMWF Forecast User Guide*. ECMWF, Reading, 05/2018 2018. <p> Replaces previous editions that were available as PDF documents.</p>.
- [76] Sebastian Schubert and Valerio Lucarini. Dynamical analysis of blocking events: spatial and temporal fluctuations of covariant lyapunov vectors. *Quarterly Journal of the Royal Meteorological Society*, 142(698):2143–2158, 2016.
- [77] Valerio Lucarini and Andrey Gritsun. A new mathematical framework for atmospheric blocking events. *Climate Dynamics*, 54(1):575–598, 2020.
- [78] Michael T. Rosenstein, James J. Collins, and Carlo J. De Luca. A practical method for calculating largest lyapunov exponents from small data sets. *Physica D: Nonlinear Phenomena*, 65(1):117–134, 1993.
- [79] Xuan Li and Ruiqiang Ding. The backward nonlinear local lyapunov exponent and its application to quantifying the local predictability of extreme high-temperature events. *Climate Dynamics*, 60(9):2767–2781, 2023.
- [80] Robin Noyelle, Pascal Yiou, and Davide Faranda. Investigating the typicality of the dynamics leading to extreme temperatures in the ipsl-cm6a-lr model. *Climate Dynamics*, 62(2):1329–1357, 2024.
- [81] Otto E Rössler. An equation for continuous chaos. *Physics Letters A*, 57(5):397–398, 1976.
- [82] Jianping Li and Ruiqiang Ding. Temporal–spatial distribution of atmospheric predictability limit by local dynamical analogs. *Monthly Weather Review*, 139(10):3265–3283, 2011.
- [83] George Datsoris and Ulrich Parlitz. *Nonlinear dynamics: a concise introduction interlaced with code*. Springer Nature, 2022.
- [84] Clio Michel and Gwendal Rivière. The link between rossby wave breakings and weather regime transitions. *Journal of the Atmospheric Sciences*, 68(8):1730–1748, 2011.

## Supplementary Information

### A Lorenz system and its stochastic version

The Lorenz-63 system [19] was originally derived from a simplified model of the atmospheric convection process and has been widely used as an example to study chaotic dynamical systems. Its governing equations can be written as:

$$\frac{dx}{dt} = \sigma(y - x), \quad (11)$$

$$\frac{dy}{dt} = x(\rho - z) - y, \quad (12)$$

$$\frac{dz}{dt} = xy - \beta z. \quad (13)$$

In this study, we adopt the classical parameters of the Lorenz system that exhibit deterministic chaos, where  $(\sigma, \rho, \beta) = (10, 28, 8/3)$ . Observational data are obtained through numerical simulation with a temporal resolution of  $dt = 0.005$  over  $10^5$  time steps.

Additionally, we test the impact of noise on our predictability index by considering the Lorenz-63 system with diffusion terms. The corresponding equations can be written as:

$$\frac{dx}{dt} = \sigma(y - x) + \eta dW_t^1, \quad (14)$$

$$\frac{dy}{dt} = x(\rho - z) - y + \eta dW_t^2, \quad (15)$$

$$\frac{dz}{dt} = xy - \beta z + \eta dW_t^3. \quad (16)$$

where  $dW_t^j$ ,  $j = 1, 2, 3$  indicate increments of three independent Wiener processes, and  $\eta$  modulates the intensity of the stochastic perturbations. In Supplementary Figure 7, we show the predictability index for the Lorenz system with stochastic perturbations, using the same numerical simulation settings as in Figure 2, with the value of  $\eta = 1$ . We note that the Supplementary Figure 7 is overall similar to Figure 2 for the five different forecasting horizons considered. However, we observe small-scale fluctuations of  $\alpha_\eta$ , which corresponds to the characteristics of the stochasticity within the system. In addition, the value of  $\alpha_\eta$  drops more rapidly on average as expected, since the stochastic nature will make the system less predictable in general.

### B The scale-dependent nature of predictability

Just like other local indices, the computation of  $\alpha_\eta$  requires a quantile parameter  $q$  that defines *recurrences*, indicating the number of *recurrences* for each state used in the analysis. For local dimension  $d$  and inverse persistence  $\theta$ , they are found to be stable within a certain range where the threshold is neither too high, making *recurrences* insufficient to fit the generalized Pareto distribution, nor too low, leading to other distributions [62]. For  $\alpha_\eta$ , although we do not need to fit the generalized Pareto distribution, we are still interested in how the value of  $q$  will affect the results.

Different values of  $q$  will result in different sizes of the neighborhood. Therefore, We interpret the predictability index derived from different  $q$  actually representing local predictability at different scales. The scale-dependent nature of predictability has been widely recognized in previous studies [35, 34, 36]. For instance, in the linear regime, the maximum Lyapunov exponent denotes predictability for dynamical systems. However, when the error is finite (outside the linear regime), this is no longer sufficient because nonlinear dynamics play a more important role in predictability.

In this paper, all the results displayed in the main text use  $q = 0.99$ , which means the closest one percent of states to the reference state are selected as *recurrences*. Figure 8 and 9 show the results for  $q = 0.98$  and  $q = 0.995$ , respectively, following exactly the same settings as Figure 2. We note that using different  $q$  values yields similar overall results, with the most prominent features being noticeable in each case. However, we also observe some differences: for larger  $q$  values ( $q = 0.995$ ), small-scale stripes on the attractor are visible, whereas for relatively smaller  $q$  values, no such patterns exist and the variation of  $\alpha_\eta$  in phase space appears smoother. This confirms the close relationship between predictability and scale, indicating that the choice of  $q$  should be made according to specific application needs.

In Figure 10, we further tested a wider range of  $q$  values for their influence on the value of  $\alpha_\eta$ . Four states at different locations on the Lorenz-63 attractor are shown in Figure 10 (a), representing the wing, near the fixed point, before lobe transition (before the intersection of the two wings), and after lobe transition (after the intersection of the two

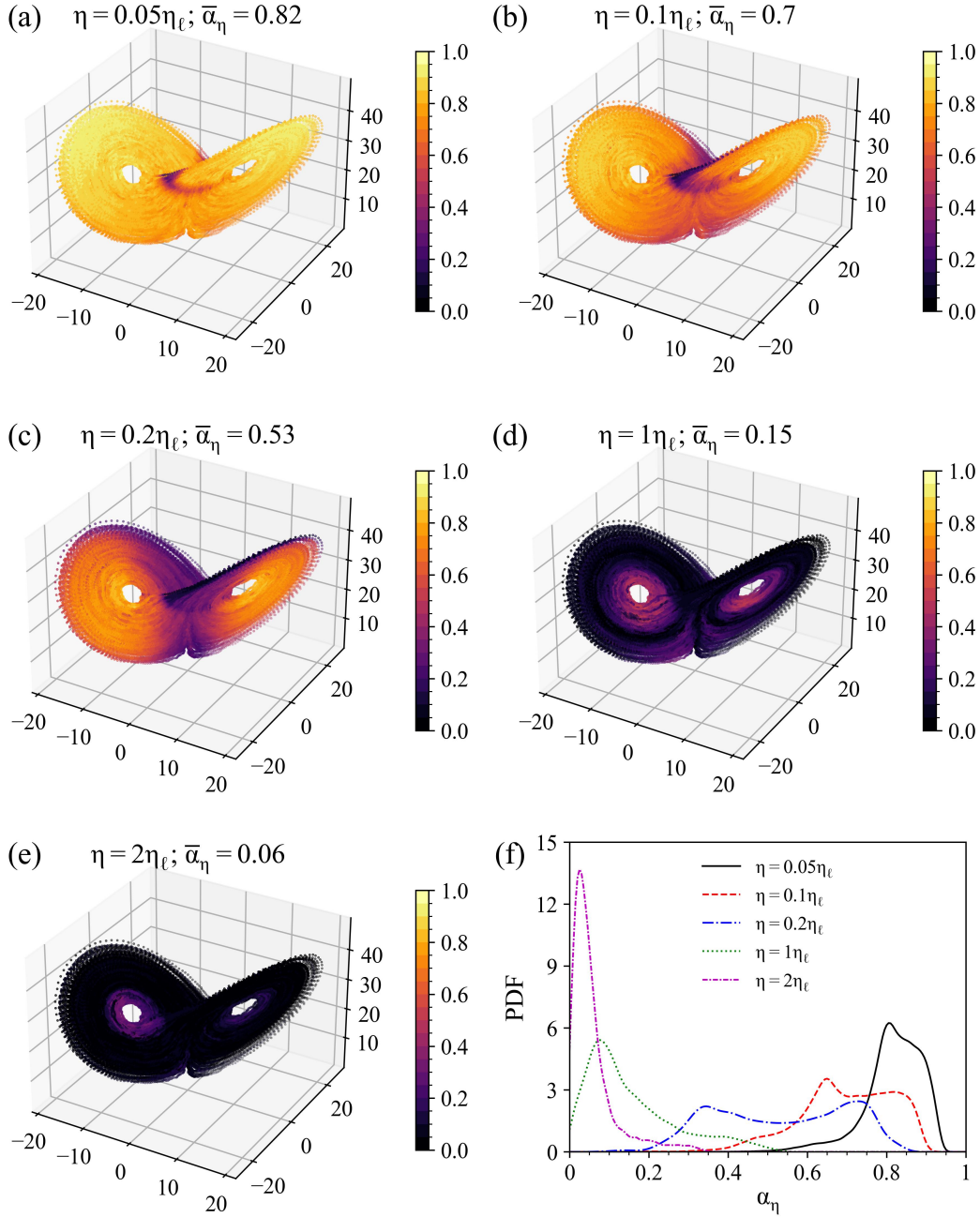


Figure 7: Distribution of  $\alpha_\eta$  at different prediction horizons for the stochastic Lorenz-63 system. Same as Figure 2, but for the stochastic version of the Lorenz-63 system.

wings). The  $\alpha_\eta$  computed from  $q$  ranging from 0.98 (2000 *recurrences* for dataset with length of  $10^5$ ) to 0.9999 (10 *recurrences*) are demonstrated in Figure 10 (b-e). We can see that although the overall differences given by different  $q$  values are not significant, there are still noteworthy distinctions that confirm the scale-dependent nature of predictability.

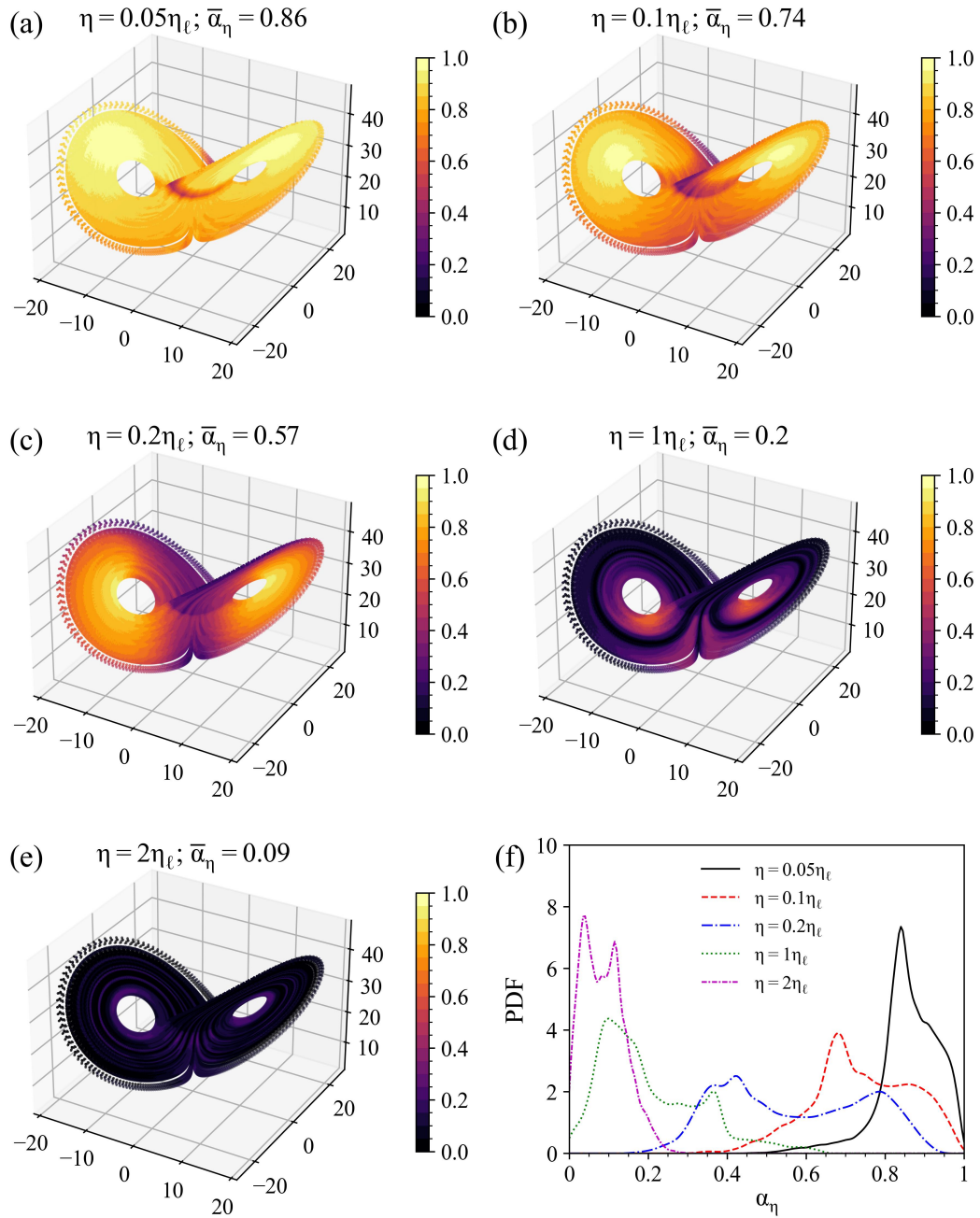


Figure 8: Comparative analysis of the impact of different quantile choices ( $q$ ) on  $\alpha_t$ . Same as Fig. 2, but for  $q = 0.98$ .

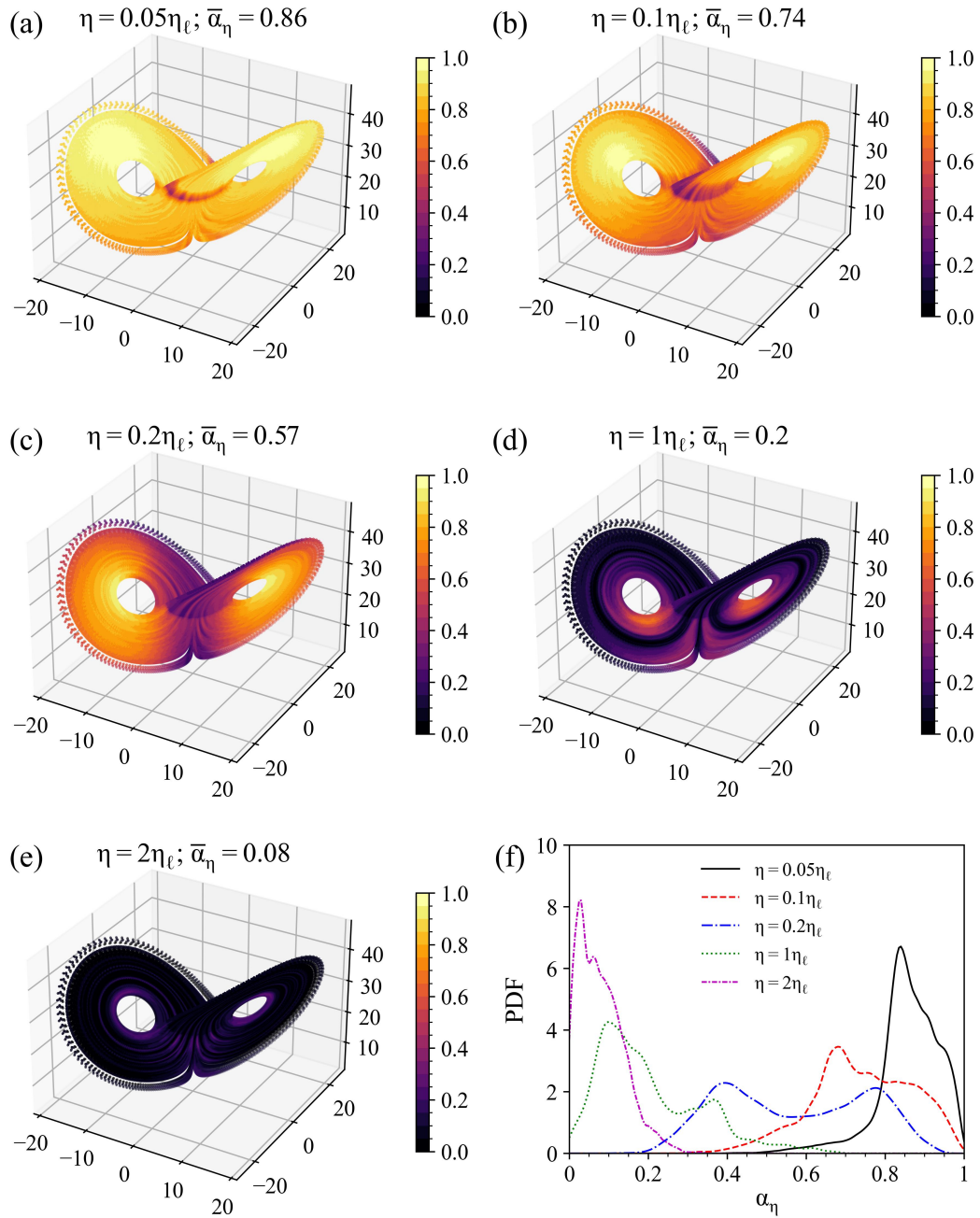


Figure 9: Comparative analysis of the impact of different quantile choices ( $q$ ) on  $\alpha_t$ . Same as Fig. 2, but for  $q = 0.995$ .

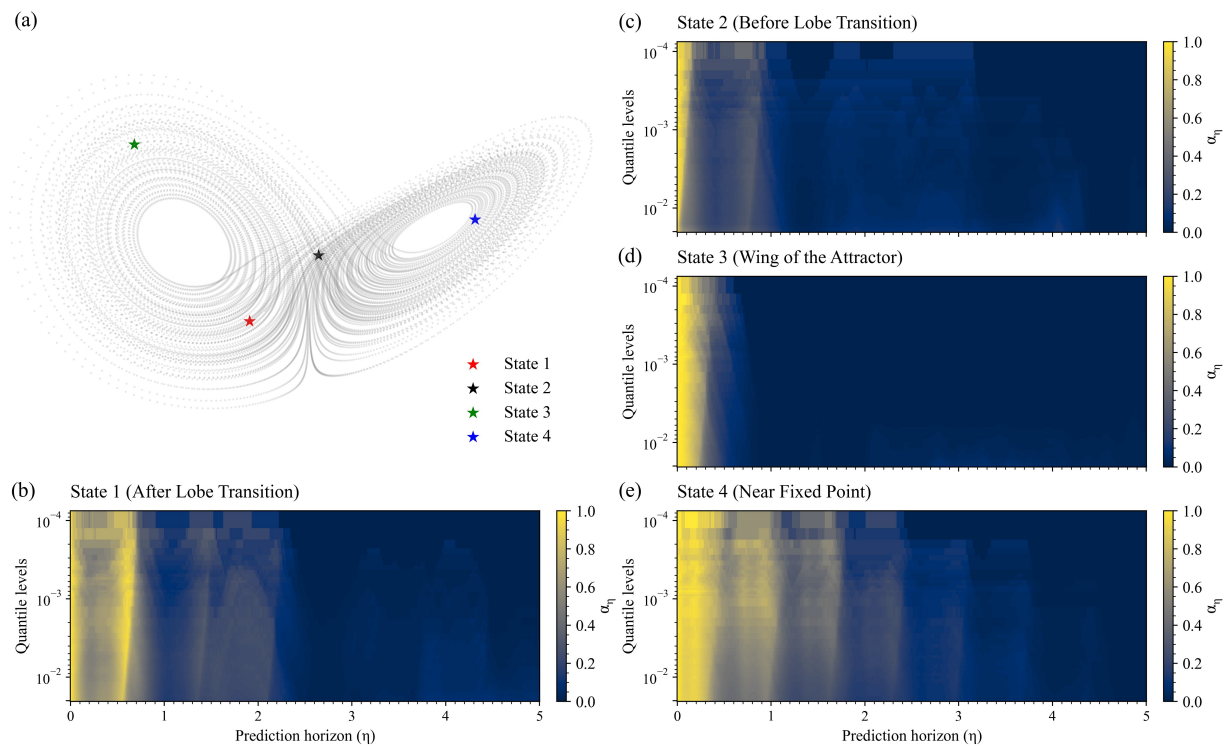


Figure 10: Predictability analysis for different  $q$  values. (a) Illustration of the locations of the states considered in the Lorenz-63 phase space. (b-e) Heatmaps of  $\alpha_\eta$  for four states located at the wing, near the fixed point, before lobe transition (before the intersection of the two wings), and after lobe transition (after the intersection of the two wings), respectively.

## C Results for other dynamical systems

We also applied our predictability index to other idealized dynamical systems with varying complexity, including the Rössler system, and the spring-slider system for laboratory earthquakes.

### C.1 Rössler system

The Rössler system is a set of three nonlinear ordinary differential equations originally introduced in 1976 [81]. Its governing equations can be written as:

$$\frac{dx}{dt} = -y - z, \quad (17)$$

$$\frac{dy}{dt} = x + ay, \quad (18)$$

$$\frac{dz}{dt} = b + z(x - c). \quad (19)$$

In this study, we adopt the classical parameters of the Rössler system that exhibit deterministic chaos, where  $(a, b, c) = (0.2, 0.2, 5.7)$ . Observational data are obtained through numerical simulation with a temporal resolution of  $dt = 0.005$  over  $10^5$  time steps.

### C.2 Spring-slider system for laboratory earthquakes

We follow the equations provided in [16] to generate the laboratory earthquakes dataset. We generated  $2 * 10^5$  time steps with  $dt = 0.01$  for the analysis.

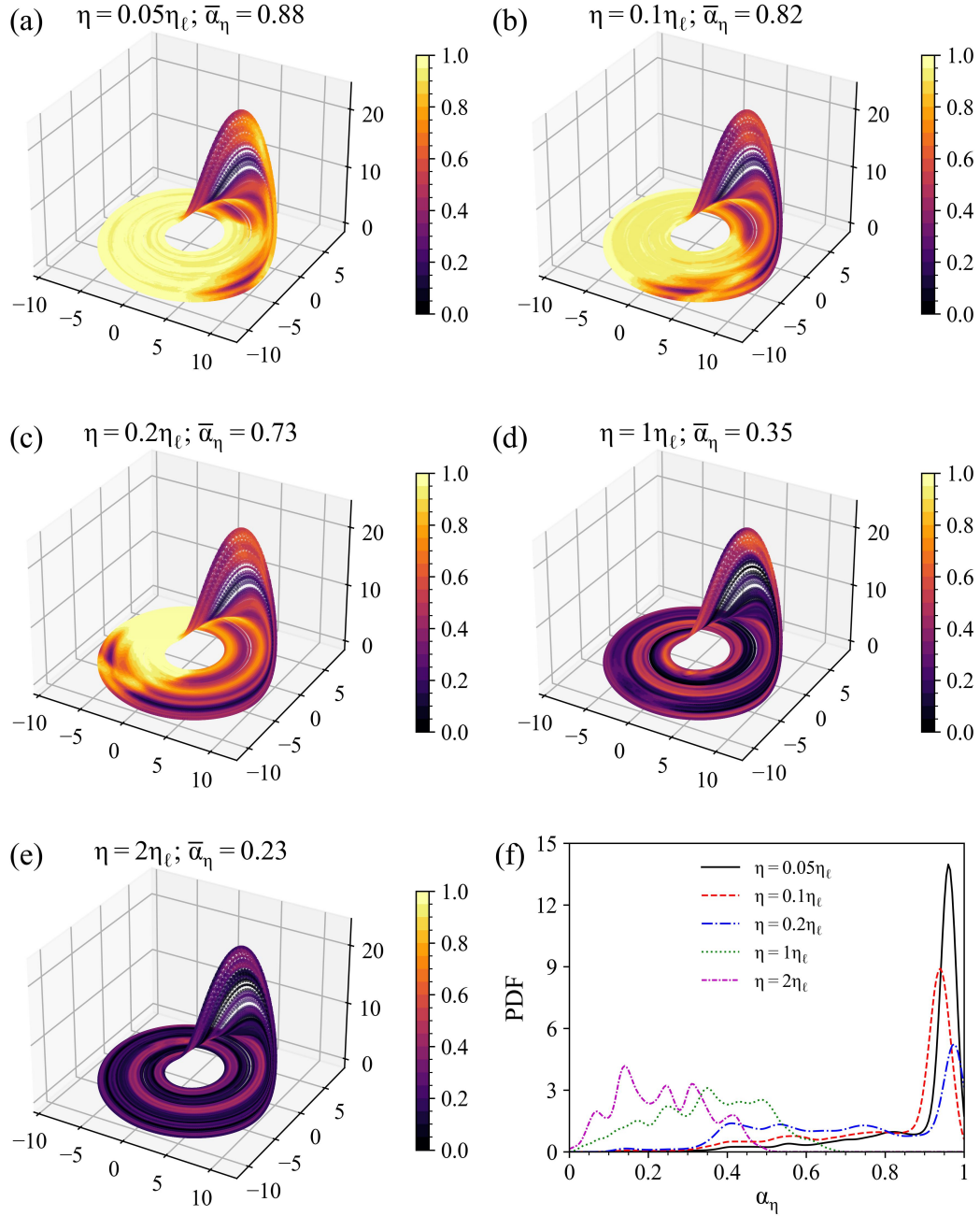


Figure 11: Distribution of  $\alpha_\eta$  at different prediction horizons for the Rössler system. Same as Figure 2, but for the Rössler system and its corresponding Lyapunov time.

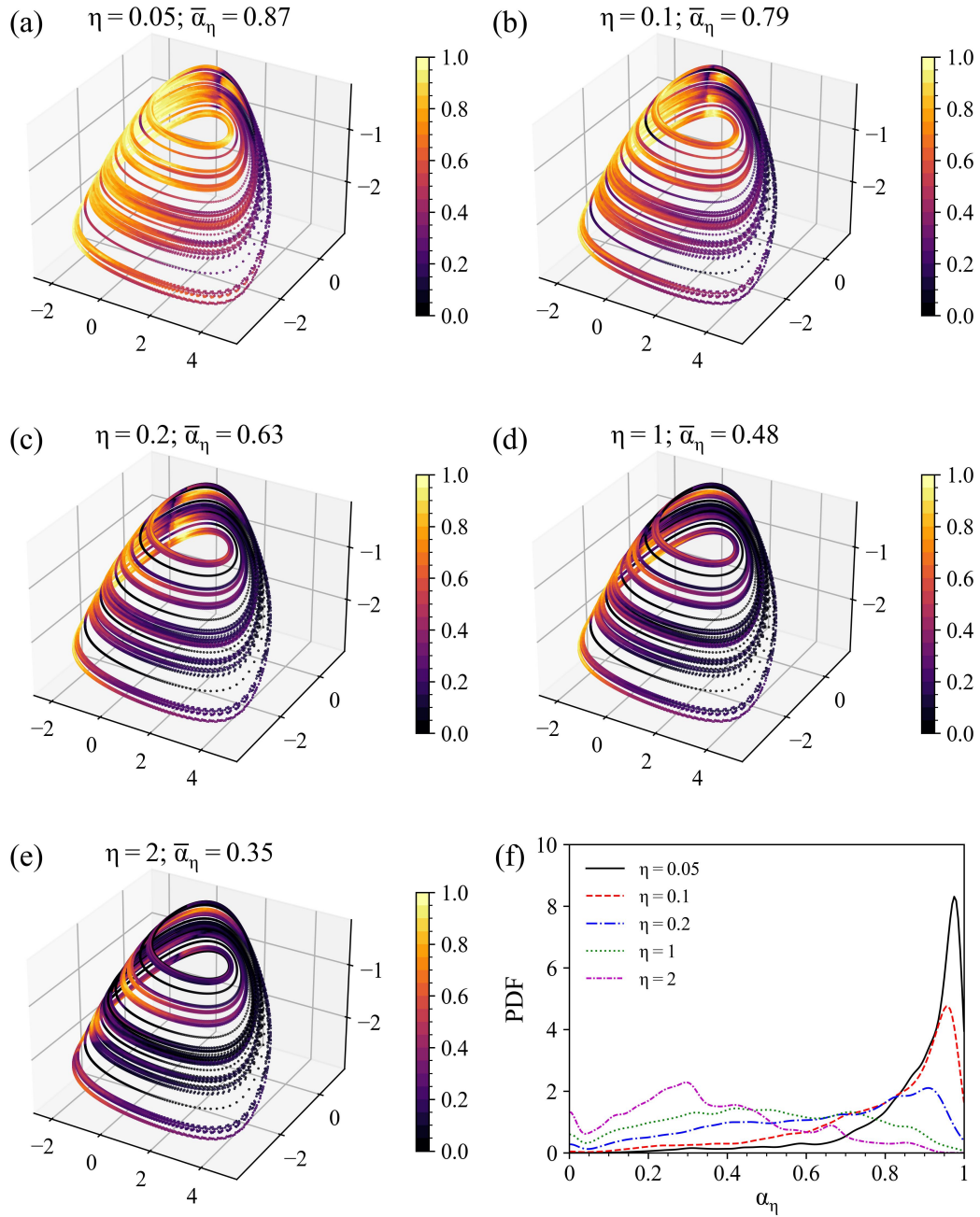


Figure 12: Distribution of  $\alpha_\eta$  at different prediction horizons for the deterministic spring-slider system. Same as Figure 2, but for the deterministic spring-slider system.

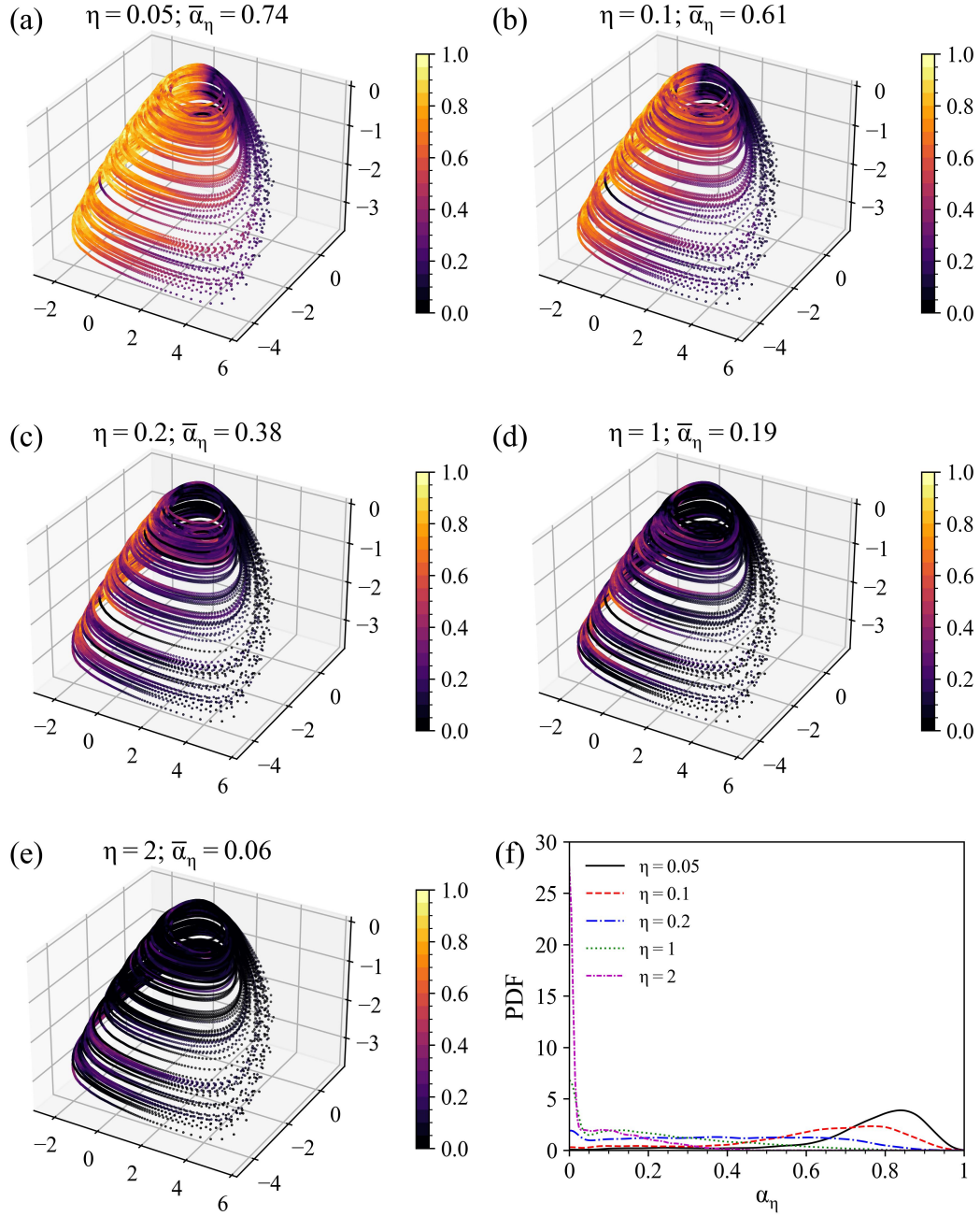


Figure 13: Distribution of  $\alpha_\eta$  at different prediction horizons for the stochastic spring-slider system. Same as Figure 2, but for the stochastic spring-slider system.

## D Comparison with Nonlinear Local Lyapunov Exponent

The Nonlinear Local Lyapunov Exponent (NLLE) was first proposed by Ding and Li in 2007 [36]. Unlike previous approaches that rely on linearized dynamics, NLLE uses the full dynamics to characterize the error growth rate without linearizing the governing equations. When the governing equations of the dynamical system is not explicitly known, they provided a method for estimating NLLE from observational data based on analogous, as shown in [82]. This index is sometimes also called the 'Local Growth Rate', with an open-source implementation provided in [83]. In this section, we computed NLLE using the same Lorenz-63 dataset as used in the main analysis. Figure 14 demonstrates the distribution of NLLE ( $\lambda_\eta$ ) for different  $\eta$ .

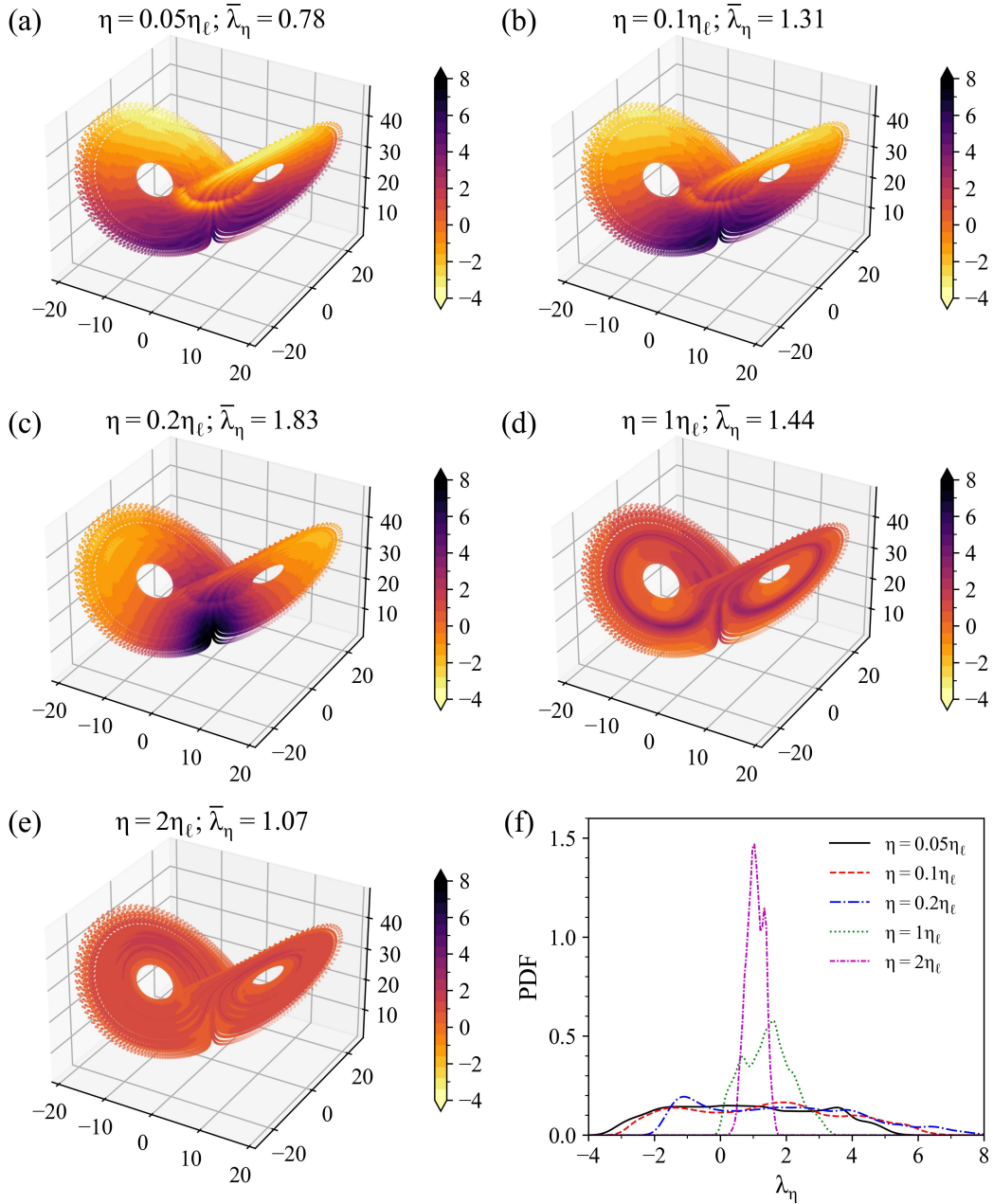


Figure 14: Distribution of NLLE at different prediction horizons for the stochastic Lorenz-63 system. Same as Figure 2, but for the Nonlinear Local Lyapunov Exponent.

## E Extension of the Predictability Index

In this paper, we introduce a new method that characterizes the local predictability of a dynamical system by applying the concept that measuring predictability can be viewed as assessing the divergence rate of nearby trajectories. This is implemented by counting the number of trajectories that evolve closely with the reference trajectory, normalized to a bounded value using the size of the neighborhood. Despite this approach demonstrating potential in analyzing local predictability, it discards information about trajectories that have left the neighborhood, whose dynamics also reflect predictability to some extent. To this end, we proposed an extension of this predictability index by weighting all the nearby trajectories by their distances to the reference trajectory.

Recall that when deriving  $\alpha_\eta$  for a given reference state  $\zeta$  and forecasting horizon  $\eta$ , we defined three groups of states: *recurrences* ( $R_{t_\zeta}$ ), *forward recurrences* ( $R_{t_\zeta}^\eta$ ) and *forward-reference-state recurrences* ( $R_{t_\zeta+\eta}$ ). Based on these three groups of states, we define the value of the original version  $\alpha_\eta$  as follows:

$$\alpha_\eta(\zeta) = \frac{|R_{t_\zeta}^\eta \cap R_{t_\zeta+\eta}|}{|R_{t_\zeta}|} \quad (20)$$

To extend this index, we first track the distances of all states belonging to *forward recurrences* ( $R_{t_\zeta}^\eta$ ) to the reference trajectory as  $D$ :

$$D = \left\{ \text{dist}(x(t), x(t_\zeta + \eta)) \quad \forall x(t) \in R_{t_\zeta}^\eta \right\}. \quad (21)$$

where the dist function can be any distance metric, but we only consider L2 norm in this study.

Next, we also record the distances of states that belong to the intersection of *forward recurrences* ( $R_{t_\zeta}^\eta$ ) and *forward-reference-state recurrences* ( $R_{t_\zeta+\eta}$ ) to the reference trajectory. We denote these distances as  $D'$ :

$$D' = \left\{ \text{dist}(x(t), x(t_\zeta + \eta)) \quad \forall x(t) \in R_{t_\zeta}^\eta \cap R_{t_\zeta+\eta} \right\}. \quad (22)$$

Based on these distances, we further define the extension of the index  $\alpha_\eta^*(\zeta)$  as:

$$\alpha_\eta^*(\zeta) = \frac{\sum_{d' \in D'} \phi(d')}{\sum_{d \in D} \phi(d)} \quad (23)$$

where  $\phi$  can be a custom positive function used to make the extension focus on different aspects, as further explained later. Since  $D'$  is a subset of  $D$ , the values of  $\alpha_\eta^*$ , like  $\alpha_\eta$ , are also defined to lie within the range of 0 to 1. Specifically, we note that the original  $\alpha_\eta$  can be viewed as a special case of the extended index  $\alpha_\eta^*$  when  $\phi(x) = x^0$ , meaning that all trajectories are not weighted by their distances to the reference trajectory.

In Figure 15 and 16, we show the results of  $\alpha_\eta^*$  using  $\phi(x) = x^{-1}$  and  $\phi(x) = x$ , respectively. For these two different  $\phi(x)$ , the results are generally similar to those obtained when  $\phi(x) = 1$ , although they show noticeable differences in the details. When  $\phi(x) = x^{-1}$ ,  $\alpha_\eta^*$  decreases slowly as the forecasting horizon increases, whereas the opposite holds for  $\phi(x) = x^1$ . This can be explained as  $\phi(x) = x^{-1}$  assigns higher weights to the close neighbors, while  $\phi(x) = x^1$  assigns higher weights to the states that are farther away. This means we can selectively define  $\phi$  based on the needs of different tasks. For instance, in some cases, we may be particularly interested in fast diverging trajectories, making  $\phi(x) = x^1$  a more suitable choice.

To sum up, this extension uses distances as weights, incorporating more information compared to the original  $\alpha_\eta$  which relies on binary values. It also estimates local predictability, and with the extensible nature provided by the weighting function  $\phi$ , it offers additional information for analysis.

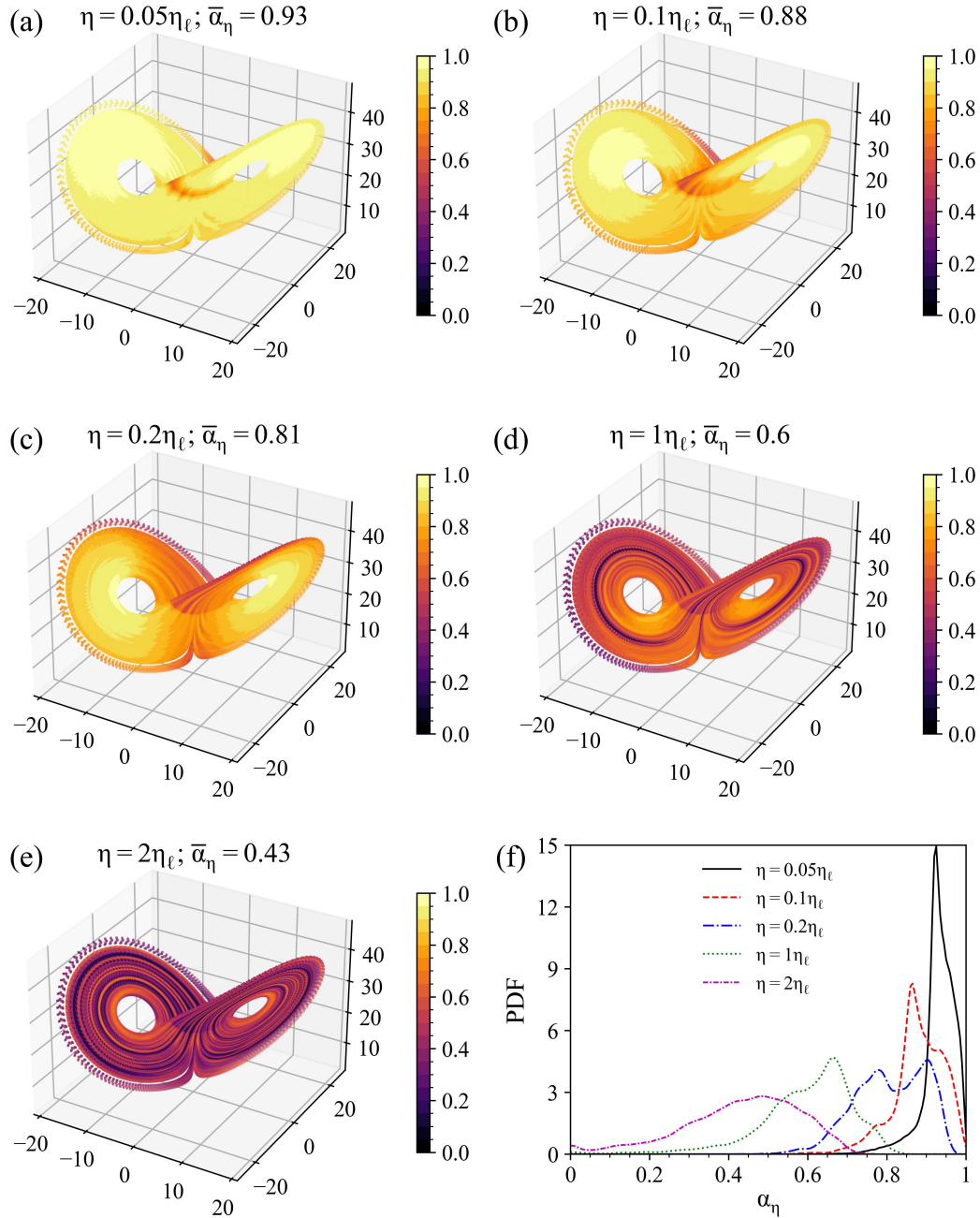


Figure 15: Distribution of  $\alpha_\eta^*$  at different prediction horizons for the Lorenz-63 system, with  $\phi(x) = x^{-1}$ . Same as Figure 2, but for the extension of the predictability index.

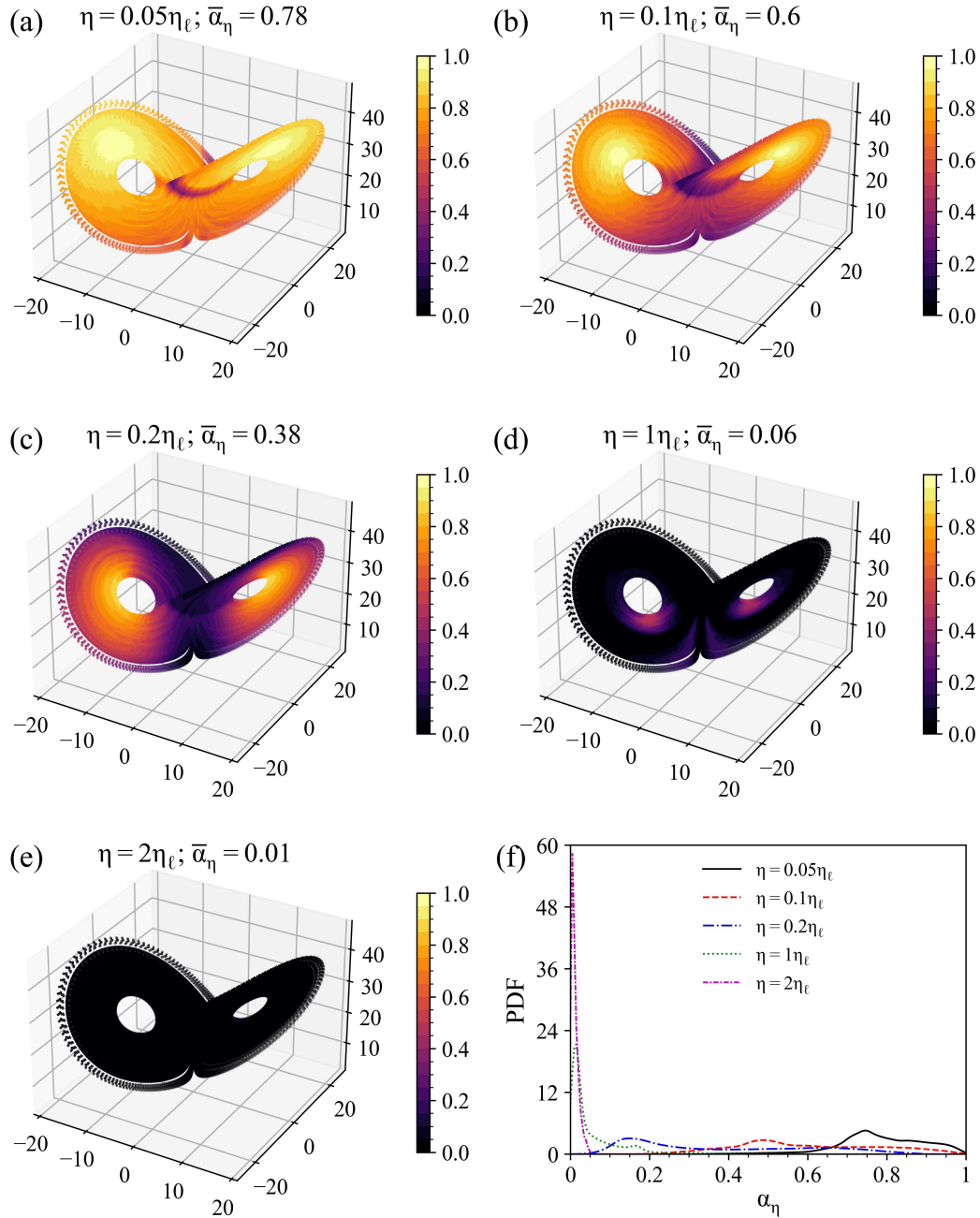


Figure 16: Distribution of  $\alpha_\eta^*$  at different prediction horizons for the Lorenz-63 system, with  $\phi(x) = x$ . Same as Figure 2, but for the extension of the predictability index.

## Definition of North Atlantic Wintertime Weather Regimes

The definition of weather regimes is adapted from [74], focusing on the wintertime (DJFM) 500 hPa (Z500) in the Euro-Atlantic sector (80°W to 50°E, 22.5°N to 70°N). The weighted Z500 daily anomaly data is decomposed using EOF analysis, retaining the 14 leading modes (accounting for approximately 90% of the variance) to speed up the computation. The climatology is computed as the calendar day mean field of Z500 from 1979 to 2022, based on a centered 15-day window, while the weight is applied to the data as a cosine function of the latitude. The k-means clustering algorithm is then applied to the principal components, resulting in four weather regimes, whose centroids are demonstrated in Fig. 17. Next, we compute the normalized projection of each daily Z500 anomaly field onto the cluster centroid, which has been termed the Weather Regimes Index (IWR) in previous studies [84]. Here, we aim to analyze the predictability of established weather regimes; therefore, we require that the Weather Regimes Index (IWR) remains above 1.0 for at least 5 days to classify a state as belonging to a weather regime. States that are not allocated to any weather regime are classified as "no regime".

## Real-time Predictability Analysis

In certain scenarios, such as weather forecasting, real-time predictability analysis is important for evaluating and informing the operational forecast system. However, the computation of  $\alpha_\eta$  rely on the future trajectory of the reference state  $\zeta'$ , therefore hindering direct real-time applications. As shown in Equation 9 in the main text, we propose a proxy that do not rely on the future information of the reference state. The idea of this proxy stems from the fact that the predictability index represents local predictability in the phase space. Therefore, we can use the average predictability of the neighboring states of  $\zeta'$  to represent its predictability.

An example of a real-time application is presented using the Lorenz-63 system, following the same numerical simulation scheme as other experiments in this study. We assume that we have  $10^5$  time steps as historical observations, and their corresponding  $\alpha_\eta$  have already been computed, as shown in Fig. 18 (b,d,f). Meanwhile, we also assume there are 2000 states not present in the historical observations, which are used to simulate real-time unseen states in an operational forecast system. Figure 18 (a,c,e) shows the predictability proxy for the unseen states. By comparing the results with the reference  $\alpha_\eta$ , we note that the proposed proxy can effectively capture the features of predictability, regardless of the region in phase space or the forecasting horizon. Specifically, the low predictability near the lobe transition region is in Fig.18 (a,c), and the high predictability region near the fixed point in Fig.18 (e) are both well reflected. Although this application is a rather simple case, we anticipate its application in other operational forecast systems.

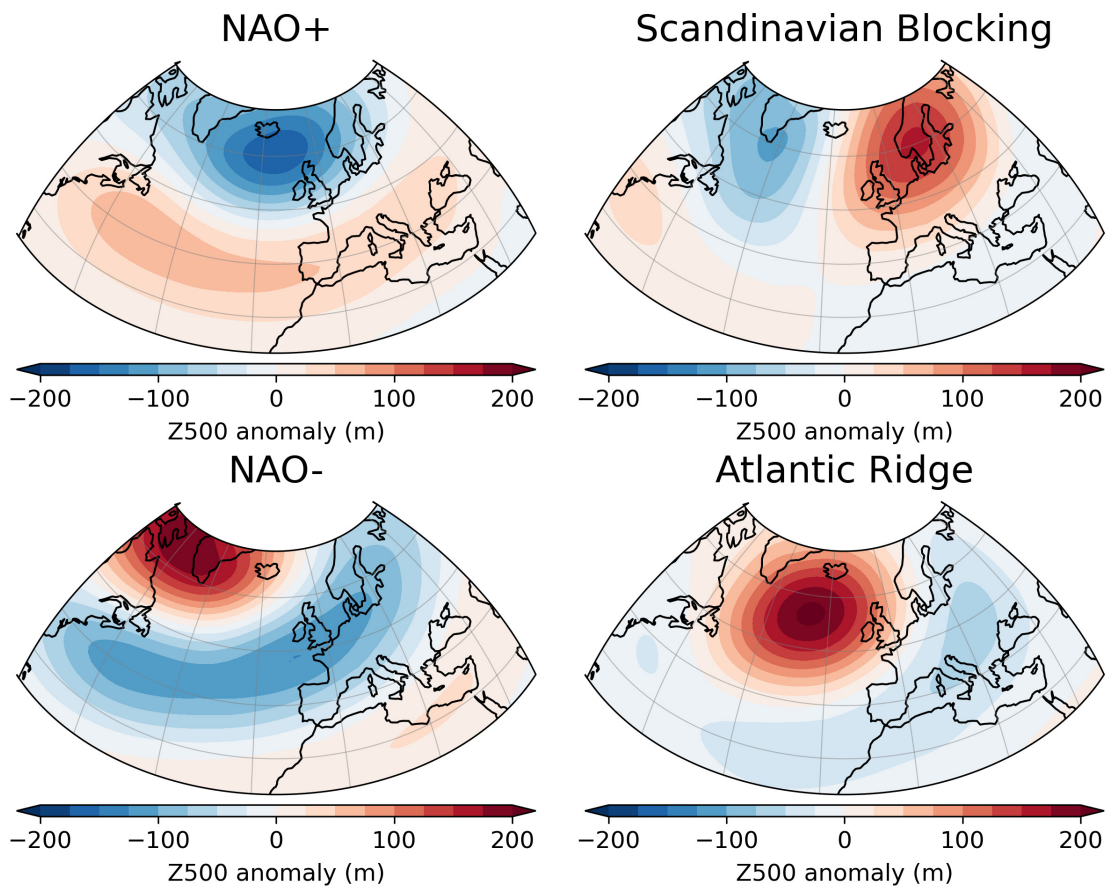


Figure 17: Composite Z500 anomaly maps for the four weather regimes in the North Atlantic-Europe region.

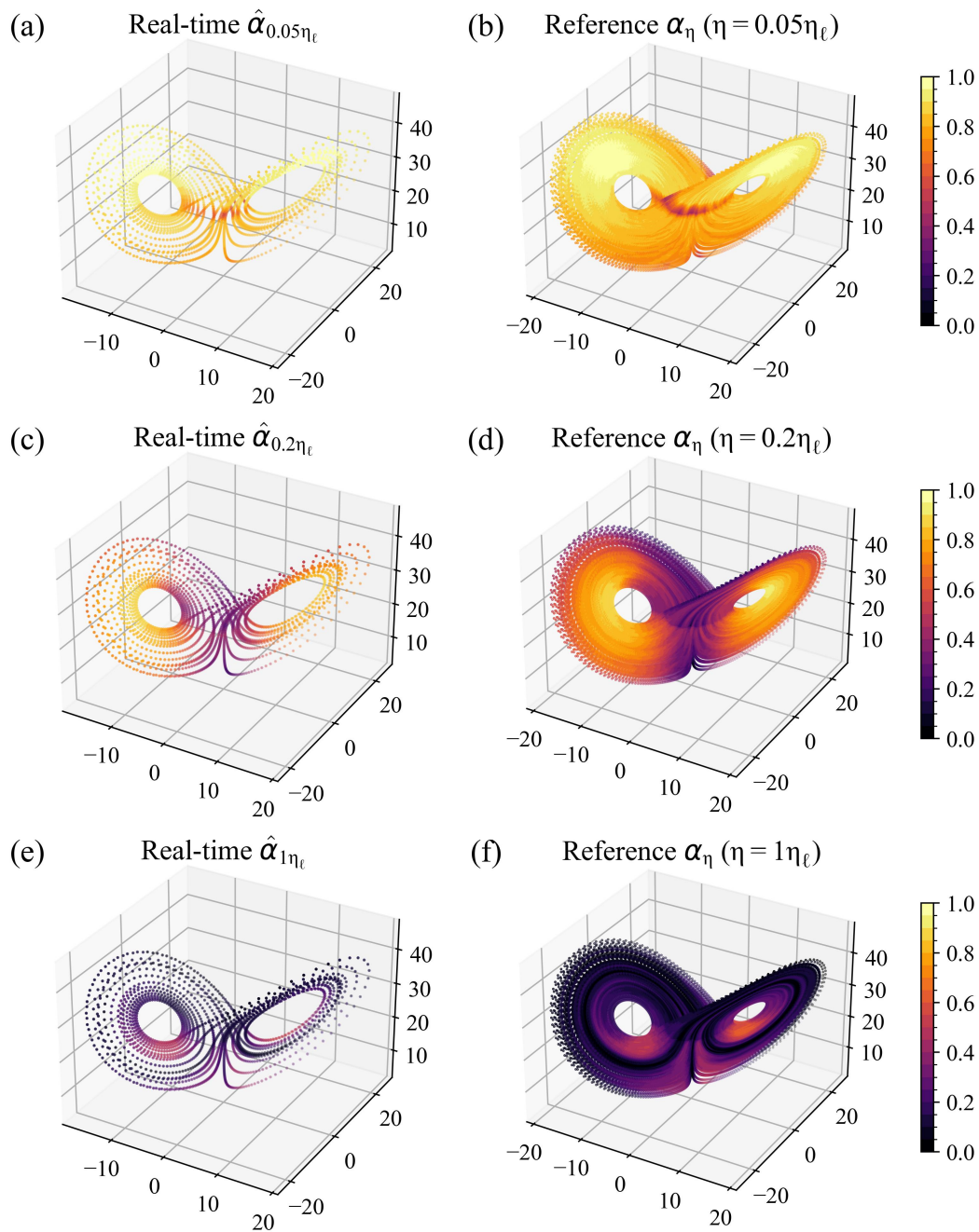


Figure 18: Real-time predictability analyses for the Lorenz system. (a,c,e) 2000 unseen Lorenz-63 states colored according to the predictability index proxy  $\hat{\alpha}_\eta$ , presented across three different forecasting horizons:  $0.05\eta_\ell$  (a),  $0.2\eta_\ell$  (c), and  $1\eta_\ell$  (e). Panels (b), (d), and (f) display the reference  $\alpha_\eta$ , as in 2 (a), (c), and (d).